2016

Implications of Hf-Nd Isotopes in West Philippine Basin Basalts for the Initiation and Early History of the Izu-Bonin-Mariana Arc

Benjamin D. Hocking
University of South Carolina

Implications of Hf-Nd Isotopes in West Philippine Basin Basalts for the Initiation and Early History of the Izu-Bonin-Mariana Arc

by

Benjamin D. Hocking

Bachelor of Arts
State University of New York at Geneseo, 2012

Submitted in Partial Fulfillment of the Requirements

For the Degree of Master of Science in

Geological Sciences

College of Arts and Sciences

University of South Carolina

2016

Accepted by:

Gene Yogodzinski, Director of Thesis

Michael Bizimis, Reader

Andrew Leier, Reader

Lacy Ford, Senior Vice Provost and Dean of Graduate Studies

Abstract

Drilling at Site U1438, located immediately west of Kyushu-Palau Ridge (KPR), the site of IBM subduction initiation, penetrated 1,460 m of volcaniclastic sedimentary rock and 150 m of underlying basement. Biostratigraphic controls indicate a probable age for the oldest sedimentary rocks at around 55 Ma. This is close to the 48-52 Ma time period of IBM subduction initiation, based on studies in the forearc. There, the first products of volcanism are tholeiitic basalts termed FAB (forearc basalt), which are more depleted than average MORB and show subtle indicators of geochemical enrichment due to subduction. Site U1438 basement basalts share many characteristics with FABs, including primitive major elements (high MgO/FeO*) and trace element patterns more depleted than those of normal MORB with respect to Nd, Sm, Lu, and Hf abundances, as well as Lu-Hf, Nd-Lu, and Sm-Nd ratios. Hf-Nd isotopes for Site 1438 basement basalts show a significant range of compositions from ε_{Nd} of 7.0 to 9.5 and ε_{Hf} of 14.5 to 19.8 (present-day values). The data define a well-correlated array in Hf-Nd isotope space with relatively radiogenic Hf compared to Nd, which indicates an Indian Ocean-type MORB source. The dominant signature, however, with ε_{Hf} >16.5, is more radiogenic than most Indian MORB. The pattern through time is from more-to-less radiogenic and more variable Hf-Nd isotopes within the basement section. This pattern culminates in basaltic andesite sills, which intrude the lower parts of the sedimentary section. The sills have the least radiogenic compositions measured so far (ε_{Nd} ~6.6, ε_{Hf} ~13.8), and are similar to

those of boninites of the IBM forearc and modern IBM arc and reararc rocks. The pattern within the basement suggests modest enrichment of a depleted Indian MORB source over time. These results, combined with additional new Hf-Nd isotope data from ocean drilling sites 1201 and 447, which are also located immediately west of the KPR, indicate that FAB geochemistry was produced not only in the forearc, but also in backarc locations (west of the KPR) at the time of subduction initiation. The data indicate that initiation of IBM subduction was in an extensional setting by seafloor spreading-type processes immediately prior to, and contemporaneous with, initial construction of the KPR. These processes fit the model of spontaneous subduction initiation as proposed by Stern (2004 – Earth & Planetary Science Letters), wherein a change in motion causes a plate to founder and sink below another plate, possibly along a transform boundary or other zone of weakness.

Table of Contents

List of Tables

List of Figures

Chapter 1

Introduction

Although subduction boundaries are a key part of modern plate tectonic theory, the mechanisms by which subduction is initiated, and the early development of volcanic arcs remain poorly understood. Stern (2004) proposed two basic models for subduction initiation, which he referred to as induced and spontaneous. Induced subduction occurs when two plates are forced together causing a collision and resulting in the more dense plate being thrust beneath the more buoyant. All modern subduction systems are believed to be examples of the induced subduction model. One generally accepted mechanism for induced subduction is the idea of polarity reversal (McKenzie, 1969; Cooper and Taylor, 1985; Wang et al., 2015). Spontaneous subduction occurs when a change in motion causes a plate to founder, along either a transform boundary or passive margin. In this case subduction is initiated without collision (Stern, 2004). In both models, once the initial offset of the plates occurs, the edge of the more dense plate is weighed down by mass wasting from the over-riding plate (Stern, 2004). Once the subducting plate develops a downward dip, it will begin to sink through the less dense mantle under its own weight, thereby creating a self-sustaining subduction boundary (Gurnis et al., 2004), resulting from the slab-pull affect (Forsyth and Uyeda, 1975).

The Izu-Bonin-Mariana (IBM) arc along the eastern edge of the Philippine Sea Plate (Fig. 1.1) is an ideal place to study the genesis, and early development of a subduction system, because it is a non-accreting margin where sediment cover is

relatively thin (Huene and Scholl, 1991). Most previous work on the early history of the IBM arc focused on the forearc on island exposures and along the inner trench wall where the earliest products of arc volcanism are accessible (Cosca et al., 1998; DeBari et al., 1999; Reagan et al., 2010, Ishizuka et al., 2011a).

Another opportunity to study the early history of IBM volcanism is the Kyushu-Palau Ridge (KPR), a remnant arc, and the site of IBM subduction initiation, which occurred in the time period 48-52 Ma (Ishizuka et al., 2011a; Fig. 1.1). Taylor and Goodliffe (2004) suggested that the Amami-Sankaku Basin, just west of the KPR (Fig. 1.1) was probably Cretaceous-age oceanic lithosphere of a type that must have served as the foundation upon which the IBM arc was constructed. Drilling in the Amami-Sankaku Basin was eventually carried by International Ocean Discovery Program (IODP) Expedition 351, at Site 1438 in June-July 2014 (Fig. 1.1). Drilling at Site 1438 reached a depth of ~1600 mbsf, and penetrated 150 meters of igneous basement (Fig. 1.2). Paleomagnetic, biostratigraphic and heat-flow data indicate that basement underlying the Amami-Sankaku Basis is early to middle Eocene in age, and so was formed at approximately the time of IBM subduction initiation at 48-52 Ma (Ishizuka et al., 2011a; Fig. 1.3), and so not significantly before subduction began (Arculus et al., 2014). This surprising result implies that basement recovered at Site 1438 cannot be the oceanic foundation upon which the IBM arc was constructed, but does provide an opportunity to study the earliest stages of IBM volcanism in a location immediately behind the site of subduction initiation at the KPR (Fig. 1.1).

For this study, Hf and Nd isotope ratios from basement basalts, and andesite sills recovered at from IODP Site 1438 were analyzed and compared to similar aged rocks in

the IBM forearc, in order to gain a better understanding of the mantle source for the earliest products of subduction initiation. Hafnium and Nd isotopes were also collected from basement basalts at ODP Site 1201 and DSDP Site 447 to produce parallel data sets from locations in the KPR backarc in order to determine the evolution of the mantle source early in the process of arc initiation (Arculus et al., 2015; Fig. 1.1). Hafnium and Nd were selected because they are well suited to the study of the geochemical development of the early arc, because they are resistant to seawater alteration, and generally will record the signature of magma source (Staudigel et al., 1995; Kelley et al., 2003; Thompson et al., 2008; Chauvel et al., 2009).

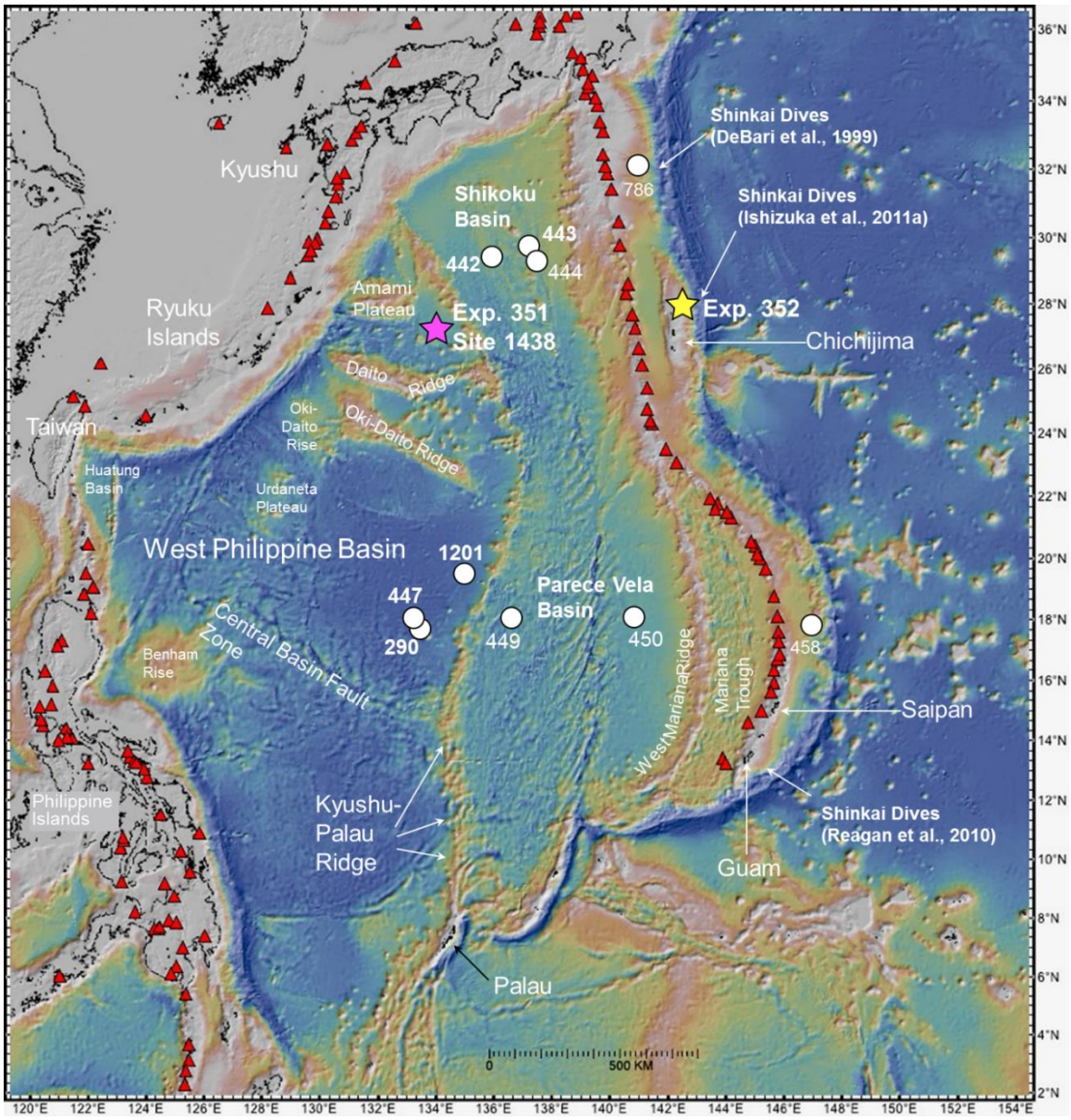

Figure 1.1 Map of the western Pacific region, showing the West Philippine Basin and Izu-Bonin-Mariana (IBM) subduction system and other locations mentioned in the text. Pink and yellow stars mark the locations of IODP Expeditions 351 and 352. White dots are locations of previous ocean drilling legs (DSDP and ODP) relevant to the proposed work. Red triangles mark the locations of active, emergent volcanoes from the Smithsonian Global Volcanism database.

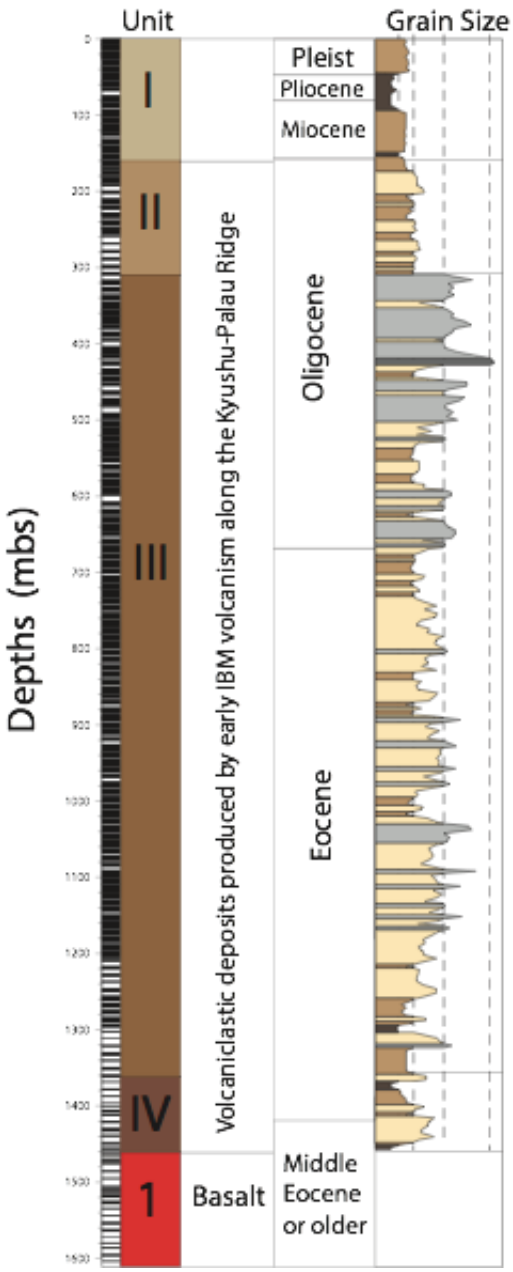

Figure 1.2 Simplified composite stratigraphic column, summarizing drilling results from IODP Expedition 351, Site 1438 (Arculus et al., 2014). Unit I is primarily unconsolidated mud with tephra. Igneous rocks of Unit IV occur approximately 50 m above the contact with basement (too small to show at this scale). Bar code on the left indicates core recovery.

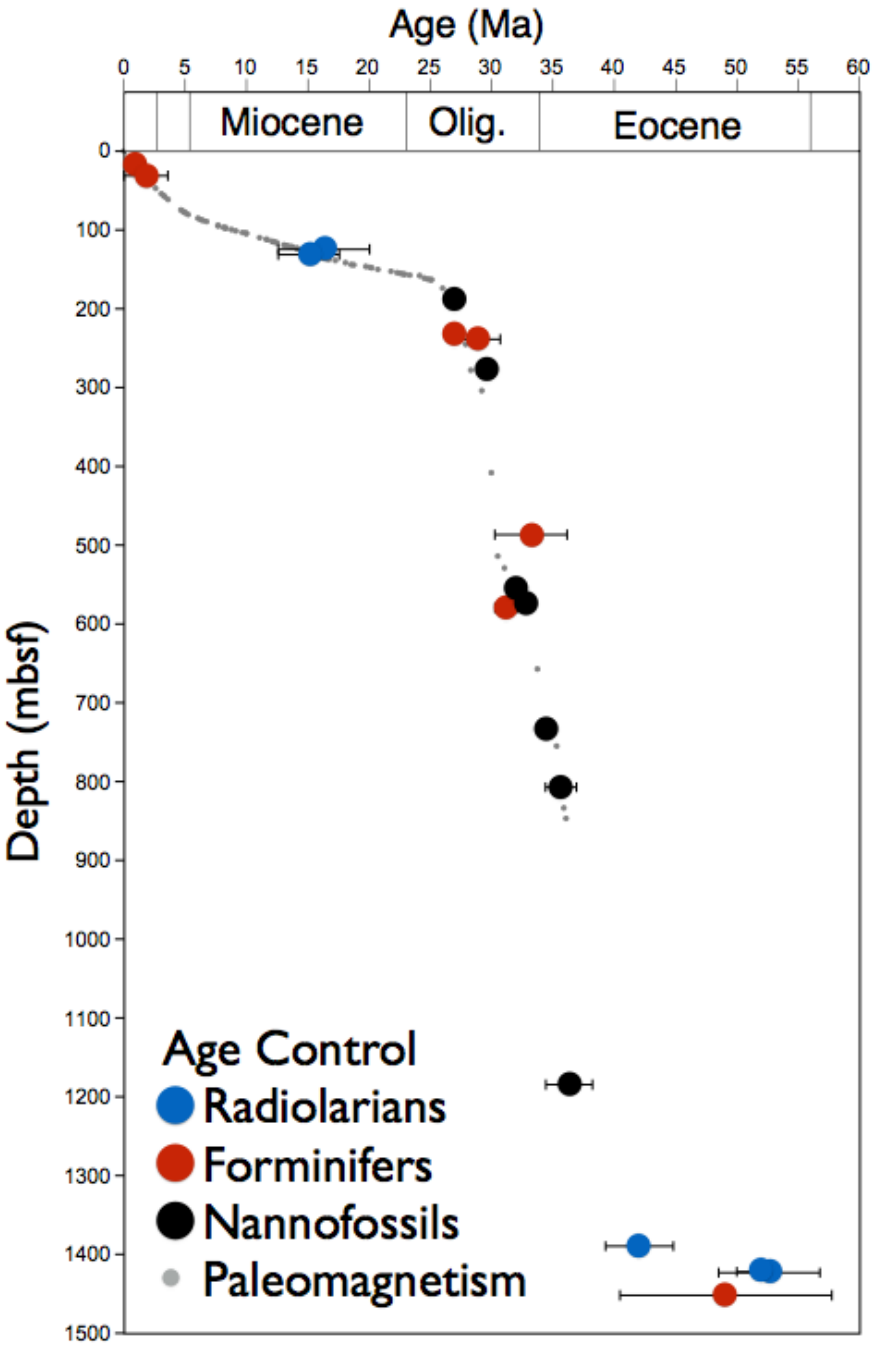

Figure 1.3. Shipboard data showing age vs depth for Expedition 351 drilling, showing the extent of biostratigraphic and paleomagnetic control over the ages of Cenozoic sediment and sedimentary rocks (Arculus et al., 2014). These results are consistent with shipboard heat flow measurements, which together, indicate that the oldest sedimentary rocks and underlying basement are likely Eocene in age, and not Cretaceous, as was thought prior to the expedition.

Chapter 2

Geologic Setting and Results of Site 1438 Drilling

Site 1438 is located approximately 75 km west of the KPR (Fig. 1.1), which marks the site of subduction initiation in the IBM system, which occurred 48-52 Ma (Sutter and Snee, 1980; Ishizuka et al., 2011b). At approximately 25 Ma, slab rollback led to the opening of the Parece-Vela and Shikoku rift basins (Fig. 1.1). This process has continued to the present, with the eventual opening the Mariana Trough just west of the modern plate boundary beginning in the Miocene (Hickey-Vargas et al., 2008). Samples recovered from the length of the KPR produce consistent minimum ages of 25 Ma, and show no significant geochemical variation through time or along-strike. These results indicate that rifting in the Parece-Vela and Shikoku basins occurred contemporaneously along the entire KPR, which experienced simultaneous cessation of volcanism at approximately 25 Ma (Kobayashi and Nakada, 1978; Ishizuka et al., 2011b).

Prior to drilling at Site 1438, and as mentioned above, the KPR was thought to be built on pre-existing Cretaceous oceanic lithosphere along the eastern margin of the West Philippine Basin. The West Philippine Basin is composed of both depleted MORB, created on the eastern side of the basin by spreading along the now extinct Central Basin Fault (active 40 to 60 Ma), as well as OIB-like basalts from hotspot activity (25-60 Ma) on the western side of the basin, forming the Benham Rise and Urdaneta Plateau (Seno and Maruyama, 1984; Deschamps and Lallemand, 2002; Hickey-Vargas et al., 2006). Spreading along the Central Basin Fault seems to be contemporaneous with the onset of

IBM arc volcanism, so the first eruptions of the IBM system may not be preserved near the fault, and may only be present at the northern and southern extremes of the KPR (Ishizuka et al., 2011b).

Site 1438 is located near the northernmost end of the KPR in the Amami-Sankaku basin in what appears to be the oldest part of the Philippine Sea Plate, the Cretaceous Ridge Complex (Fig. 1.1). The Cretaceous ridges, which intersect the KPR at a high angle, include the Amami Plateau, the Daito Ridge, and the Oki-Daito Ridge (Fig. 1.1). Early studies by Karig et al. (1975) determined that the ridges were part of an island arc system in the late Cretaceous or Paleocene, which was rifted prior to initiation of IBM subduction. Later studies by Ishizuka et al. (2011b) measured Cretaceous $^{40}Ar/^{39}Ar$ ages of 116-118 Ma for basalts collected at the intersection of the Daito Ridge and KPR. This led multiple authors to conclude that the basement of the Cretaceous Ridge Complex significantly pre-dated volcanism along the KPR (Taylor and Goodliffe, 2004; Ishizuka et al., 2011b; Arculus et al., 2015). Thus drilling at Site 1438 was undertaken with the initial goal of sampling the oceanic lithosphere upon which the IBM arc was constructed.

Drilling at Site 1438 recovered 1,461 m of sediment and sedimentary rock overlying oceanic basement. The sedimentary part of the section was divided into four geologic units (I-IV, Fig. 1.2). Unit I is composed of unconsolidated mud and ooze with interspersed layers of volcanic ash. Units II-III are volcanoclastic sedimentary rocks, mainly tuffaceous mudstones and fine sandstones, with some course tuffaceous sandstones and breccias, which are thought to have been produced by volcanism along the KPR (Fig. 1.2). Unit IV is Eocene in age, based on biostratigraphic constraints, and appears to have formed from products of early IBM volcanism. Unit IV is composed of

radiolarian-bearing mudstones, medium to coarse sandstone, breccia-conglomerate, and tuffaceous siltstone and mudstone (Arculus et al., 2014). Unit IV is of particular interest, not only because it is the oldest sediment recovered at Site 1438, and because it is intruded by three andesitic sills, located ~50 m above basement contact.

Basement at Site 1438 (Unit 1 on Fig. 1.2) consists of 150 m of fine-grained and geochemically depleted tholeiitic basalt. The minimum age of the basement is likely Middle Oligocene to Early Eocene based on biostratigraphic constraints (Arculus et al., 2014). Sedimentation rate (51-64 Mya), and thermal conductivity measurements (40-60 Mya) support the conclusion that the basement is, surprisingly, not Cretaceous, as was originally thought (Arculus et al., 2015; Fig. 1.3). Basement basalts of Unit 1 at Site 1438 provide an outstanding opportunity to examine the earliest products of IBM volcanism, and test competing ideas about subduction initiation and the earliest history of IBM volcanism.

Chapter 3

The Protoarc, FAB, and the Early History of IBM Volcanism

Initial studies of the oldest rocks on the Bonin and other forearc islands, such as Chichijima, Guam, Palau and Saipan (Fig. 1.1), as well as studies of dredged samples from the inner trench wall, led to the conclusion that the earliest products of IBM arc volcanism were dominated by boninites (Meijer, 1980; Hickey and Frey, 1982a; Cameron et al., 1983; Bloomer and Hawkins, 1987). Drilling at DSDP Sites 458 and 459 and at ODP Site 786 in the Izu-Mariana forearc (Fig. 1.1) also recovered mostly boninites, indicating that boninitic volcanism dominated the early history of the IBM system along the entire length of the arc (Hickey and Frey, 1982a). Bloomer and Hawkins (1987) describe the boninite series as rocks varying in composition from boninite to andesite, characterized by SiO_2 of 52-68 wt.% and high MgO (>8wt.%), having low abundances of TiO_2, Al_2O_3, high field strength elements (HFSE), and rare earth elements (REE). These geochemical characteristics are widely interpreted to indicate that boninites are produced by melting of a highly depleted source or by high-degree melting, probably under hydrous conditions (Hickey and Frey, 1982b). The boninite series rocks are found stratigraphically below island arc tholeiites and andesites, which dominate later phases of IBM volcanism. Therefore, boninitic volcanism was believed for many years to represent the earliest stages of arc volcanism in the IBM system (Meijer, 1980; Hickey and Frey, 1982b; Cameron et al., 1983; Bloomer and Hawkins, 1987).

A subsequent study by DeBari et al. (1999), looking for the arc basement (the old foundation upon which the arc was built), collected samples from the inner wall of the IBM trench at ~32°N (Fig. 1.1) via Shinkai 6500 submersible dives and dredging. They identified a layer of basalt, with trace element patterns similar to, but more depleted than normal MORB located ~3000 m lower on the trench wall than the boninites drilled at ODP Site 786 (DeBari et al., 1999). The depleted compositions of these basalts were more similar to Philippine Sea Plate basalts from DSDP Site 447 just west of the KPR (Fig. 1.1), than basalts previously recovered in the IBM forearc or Neogene-age backarc spreading centers (DeBari et al., 1999). Based on this similarity, depleted basalts of the inner trench wall were interpreted as a trapped piece of the Philippine Sea Plate, separated from the eastern margin of the plate when the Shikoku and Parece-Vela basins opened after 25 Ma. (Debari et al., 1999). This interpretation implied that the layer of depleted basalt identified on the inner trench wall represented an event that preceded the onset of IBM volcanism, which was still assumed to be marked by the overlying boninites (DeBari et al., 1999).

More recent Shinkai dives carried out by Reagan et al. (2010), and Ishizuka et al. (2011a) at ~12°N, and ~28°N respectively (Fig. 1.1) both found similar horizons of depleted tholeiites beneath the boninites on the inner trench wall. These studies noted that the basalts are geochemically transitional between MORB and boninite/arc-related volcanism and indicate possible subduction related volcanism preceding the boninites, which were previously accepted as the first products of IBM volcanism. The presence of geochemically similar and distinctive basalts underlying boninites in three widely separated locations along the strike of the arc suggested a common geological and

geochemical succession for the whole IBM arc (Ishizuka et al., 2011a). These observations led to the interpretation of these basalts not as a stranded fragment of the Philippine Sea Plate (i.e., Debari et al., 1999), but as the earliest products of IBM volcanism (Reagan et al., 2010; Ishizuka et al., 2011a). Reagan et al. (2010) termed these early basalts FAB (forearc basalts) and interpreted the upward succession to boninitic volcanism as the protoarc sequence, which formed shortly following the initiation of IBM subduction. Recent $^{40}Ar/^{39}Ar$ dating of protoarc samples from the Bonin Ridge by Ishizuka et al. (2011a) has bolstered these conclusions, finding that the IBM FABs were created between 48.2 – 51.1 Ma, while boninites from the same locations had somewhat younger ages of 43.94-46.02 Ma.

Reagan et al. (2010) describe FABs as tholeiitic basalts with trace element patterns more depleted than average MORB, and with certain tracers that indicate subduction input. They noted Ti/V, which can be used as a proxy for oxygen fugacity and thus used to differentiate between mantle sources, and Yb/V measured on fresh, glassy samples (Shervais, 1982; Reagan et al., 2010). However, FABs have La/Ta and La/Nb similar to MORB and so lack the negative Ta-Nb anomaly, which is characteristic of boninites and other IBM arc volcanic rocks. Plots of εHf vs. εNd exhibit more radiogenic values for both Hf and Nd in FABs than products of active arc volcanism or MORB (Reagan et al., 2010). The goal of this study is to use the geochemistry of basement basalts from drill sites 1438, 447, and 1201 to evaluate the idea proposed by Arculus et al. (2015) that FAB-type volcanism is not confined to forearc settings, but instead, occurred over a wide swath of the IBM arc at the time of subduction initiation.

Chapter 4

Samples and Data

Following completion of Expedition 351, whole-rock major element compositions were determined by XRF on 101 samples from Site 1438 by the Japan Geological Survey. These data are primarily for basement samples of Unit 1, but andesite sills intruding sedimentary rocks of Unit IV were also included. These unpublished XRF data have been provided courtesy of O. Ishizuka in support of this study. Whole-rock Hf and Nd isotopes on a selection of these samples, which are reported in Table 4.1, were measured in the Center for Elemental Mass Spectrometry at the University of South Carolina. Analytical methods for this work are described below. Whole-rock abundances for Sm, Nd, Lu and Hf on these samples, which are also reported in Table 4.1, were determined by ICPMS at Florida International University. Partial results of the trace element analyses have been provided courtesy of R. Hickey-Vargas and are also reported in Table 4.1. New Hf and Nd isotope data for basement samples at drill sites 1201 and 447, west of the KPR (Fig. 1.1) and for FAB samples collected from the northern Izu arc at 32° N (Fig. 1.1), were also measured at the University of South Carolina under this study. These data are combined with previously published Hf-Nd isotope data and abundances for Sm, Nd, Lu and Hf and are reported in Table 4.2. Published data compiled in Table 4.2 with new results are from Savov et al. (2006), DeBari et al. (1999), Hickey-Vargas (1991) and Hickey-Vargas et al. (2006). Additional details about the data are provided in the notes to Tables 4.1 and 4.2.

Table 4.1. IODP Site 1438 Unit IV Andesites and Unit 1 Basalts

Sample ID	Depth (mbsf)	$^{143}Nd/^{144}Nd$	± 2SE †	ε_{Nd} ††	$^{176}Hf/^{177}Hf$	± 2SE †	ε_{Hf} ††	Sm	Nd	Lu	Hf	Sm/Nd	Lu/Hf	Nd/Hf	Nd/Lu	$^{143}Nd/^{144}Nd$ t = 50 Ma †††	ε_{Nd} t = 50 Ma †††	$^{176}Hf/^{177}Hf$ t = 50 Ma †††	ε_{Hf} t = 50 Ma †††
IODP Site 1438 Andesite Sills																			
1438E61R2 3-5	1406.38	0.513013	5	7.5	0.283170	6	13.6	2.46	10.3	0.23	1.08	0.24	0.21	9.56	45.0	0.512966	7.8	0.283142	13.7
1438E61R2 92-95	1407.28	0.512942	5	6.1	0.283174	4	13.7	2.46	9.43	0.26	1.11	0.26	0.24	8.49	36.1	0.512891	6.3	0.283143	13.8
1438E61R2 95-97 (scar pwd)*	1408.28	0.512979	4	6.8	0.283175	4	13.8												
1438E62R1 124-126	1411.55	0.512962	4	6.5	0.283182	3	14.0	2.76	10.5	0.24	1.01	0.26	0.23	10.4	44.5	0.512911	6.7	0.283151	14.1
IODP Site 1438 Basement Basalts																			
1438E69R1 98-101	1461.90	0.513093	6	9.0	0.283296	5	18.1	1.55	4.41	0.28	1.08	0.35	0.26	4.08	15.6	0.513024	8.9	0.283262	18.0
1438E70R2 16-19	1466.70	0.513076	4	8.7	0.283293	3	18.0	1.98	5.67	0.32	1.40	0.35	0.23	4.06	17.5	0.513007	8.6	0.283262	18.0
1438E71R1 98-101	1471.10	0.513087	5	8.9	0.283293	2	17.9	1.53	4.16	0.27	1.02	0.37	0.27	4.07	15.2	0.513014	8.7	0.283257	17.8
1438E71R3 101-104	1473.76	0.513085	11	8.9	0.283257	4	16.7	1.65	4.09	0.35	1.17	0.40	0.30	3.49	11.7	0.513005	8.6	0.283218	16.4
1438E71R3 101-104 (rep)*	1473.76	0.513080	6	8.8	0.283254	4	16.6									0.513001	8.5	0.283214	16.3
1438E72R1 145-148	1476.17	0.513087	22	8.9	0.283254	5	16.6	1.97	4.60	0.32	1.22	0.43	0.26	3.79	14.6	0.513002	8.5	0.283220	16.5
1438E73R2 123-128	1486.85	0.513036	6	7.9	0.283231	4	15.8	1.29	3.44	0.32	0.87	0.38	0.37	3.95	10.7	0.512962	7.7	0.283182	15.2
1438E74R2 21-24	1495.71	0.513056	5	8.3	0.283272	3	17.2	2.28	5.64	0.44	1.49	0.40	0.29	3.79	12.9	0.512976	8.0	0.283233	16.9
1438E75R1 81-85	1504.63	0.513080	4	8.8	0.283296	4	18.1	2.12	5.63	0.41	1.40	0.38	0.30	4.01	13.6	0.513006	8.6	0.283256	17.8
1438E75R1 81-85 (rep)	1504.63	0.513083	6	8.8	0.283297	4	18.1									0.513008	8.6	0.283258	17.8
1438E76R2 86-91	1509.10	0.513073	4	8.6	0.283285	6	17.7	1.89	4.97	0.39	1.34	0.38	0.29	3.72	12.7	0.512997	8.4	0.283246	17.4
1438E76R3 105-110	1510.75	0.513074	4	8.7	0.283296	6	18.1	1.88	5.09	0.37	1.24	0.37	0.30	4.10	13.7	0.513001	8.5	0.283256	17.8
1438E77R1 53-58	1511.36	0.513070	6	8.6	0.283293	4	18.0	2.13	5.63	0.41	1.38	0.38	0.29	4.08	13.9	0.512995	8.4	0.283254	17.7
1438E77R3 41-43	1513.60	0.513062	7	8.4	0.283278	3	17.4	1.75	4.48	0.35	1.16	0.39	0.30	3.85	13.0	0.512985	8.2	0.283238	17.1
1438E77R3 41-43 (rep)	1513.60	0.513064	5	8.5	0.283272	3	17.2									0.512987	8.2	0.283232	16.9
1438E78R2 127-130	1518.09	0.513059	9	8.4	0.283275	4	17.3	1.67	4.32	0.36	1.19	0.39	0.30	3.64	12.1	0.512982	8.1	0.283235	17.0
1438E78R4 49-53	1520.12	0.513017	14	7.5	0.283195	8	14.5	1.84	4.89	0.41	1.27	0.38	0.32	3.85	12.0	0.512942	7.3	0.283152	14.1
1438E78R4 52-53 (scar pwd)*	1520.13	0.513018	8	7.6	0.283200	3	14.7												
1438E78R4 52-53 (scar pwd, rep)*	1520.13	0.513002	6	7.3	0.283200	4	14.7												
1438E79R2 6-11	1525.55	0.513019	10	7.6	0.283191	4	14.4	1.85	4.75	0.41	1.28	0.39	0.32	3.71	11.5	0.512942	7.3	0.283148	14.0
1438E79R4 48-53	1528.75	0.513073	7	8.6	0.283292	5	17.9	2.05	5.29	0.42	1.45	0.39	0.29	3.65	12.6	0.512997	8.4	0.283254	17.7
1438E80R2 27-30	1535.27	0.513088	11	8.9	0.283279	6	17.5	2.04	4.86	0.38	1.10	0.42	0.35	4.44	12.6	0.513006	8.6	0.283232	16.9
1438E81R1 114-119	1544.07	0.513084	5	8.9	0.283269	6	17.1	2.04	5.12	0.41	1.38	0.40	0.30	3.70	12.4	0.513005	8.6	0.283229	16.8
1438E82R1 61-66	1552.64	0.513077	5	8.7	0.283284	5	17.6	1.83	4.53	0.37	1.23	0.40	0.30	3.68	12.2	0.512997	8.4	0.283244	17.3
1438E82R3 77-80	1555.49	0.513099	11	9.2	0.283275	4	17.3	1.84	4.52	0.38	1.26	0.41	0.30	3.60	12.1	0.513019	8.8	0.283236	17.0
1438E83R1 112-115	1562.54	0.513119	4	9.5	0.283277	3	17.4	1.73	4.33	0.35	1.20	0.40	0.29	3.62	12.5	0.513040	9.3	0.283238	17.1
1438E83R1 112-115 (rep)*	1562.54	0.513122	16	9.6	0.283280	8	17.5									0.513043	9.3	0.283242	17.3
1438E83R1 132-136	1562.74	0.513106	5	9.3	0.283276	6	17.4	2.18	5.46	0.39	1.30	0.40	0.30	4.20	14.0	0.513028	9.0	0.283236	17.1
1438E83R3 8-10	1564.31	0.513102	13	9.2	0.283282	4	17.6	2.10	5.25	0.40	1.35	0.40	0.30	3.90	13.2	0.513023	8.9	0.283242	17.3
1438E84R1 96-99	1572.08	0.513124	6	9.6	0.283336	3	19.5	1.19	3.04	0.28	0.83	0.39	0.34	3.67	10.8	0.513047	9.4	0.283291	19.0
1438E85R1 45-47	1579.56	0.513121	5	9.6	0.283336	3	19.5	1.25	3.15	0.28	0.83	0.40	0.34	3.79	11.1	0.513043	9.3	0.283291	19.0
1438E85R1 124-127	1580.36	0.513132	6	9.8	0.283344	6	19.8	1.22	3.06	0.29	0.92	0.40	0.31	3.31	10.7	0.513053	9.5	0.283303	19.4
1438E86R1 25-28	1585.17	0.513126	4	9.7	0.283331	6	19.3	1.22	3.06	0.28	0.83	0.40	0.33	3.68	11.1	0.513047	9.4	0.283287	18.9
1438E86R2 13-16	1586.41	0.513100	5	9.2	0.283333	4	19.4	1.33	3.24	0.30	0.90	0.41	0.34	3.60	10.7	0.513019	8.8	0.283288	18.9
1438E87R1 12-15	1594.14	0.513121	3	9.6	0.283322	4	19.0	1.22	3.02	0.28	0.90	0.40	0.31	3.35	10.7	0.513041	9.3	0.283280	18.6
1438E87R1 115-118	1595.17	0.513118	4	9.5	0.283332	3	19.3	1.61	4.12	0.35	1.02	0.39	0.34	4.03	11.8	0.513041	9.3	0.283286	18.8
1438E87R3 56-60	1596.40	0.513130	6	9.8	0.283341	6	19.7	1.55	3.90	0.32	0.94	0.40	0.34	4.13	12.1	0.513052	9.5	0.283296	19.2
1438E88R1 142-145	1604.54	0.513128	7	9.7	0.283297	4	18.1	1.69	4.16	0.37	1.22	0.41	0.30	3.41	11.3	0.513048	9.4	0.283257	17.8
USGS Standards																			
BCR-2**		0.512637	6	0.1	0.282869	5	3.0												
BHVO-2**		0.512989	5	7.0	0.283101	10	11.2												

* (scar pwd) indicates a powder created from a whole rock sample at the University of South Carolina in an agate container. (rep) indicates a repeated analysis of the same sample.

** USGS standards represent average values for all measurements taken

† Uncertainties (±) reflect within-run variation calculated as 2σ standard errors and expressed as variation in the 6th decimal place.

†† Epislon values calculated with chondritic ratios of $^{176}Hf/^{177}Hf = 0.282758$ and $^{143}Nd/^{144}Nd = 0.512630$ (Bouvier et al., 2008)

††† Age corrections to 50 Ma assume $^{176}Lu/^{177}Hf = 0.1420$ and $^{147}Sm/^{144}Nd = 0.6042$ in samples and using chondritic values for these ratios from Bouvier et al. (2008)

Table 4.2 Results from ODP Site 1201, DSDP Site 447 and Northern IBM Trench Basalts

Sample	$^{143}Nd/^{144}Nd$	± 2SE †	ε_{Nd} ††	$^{176}Hf/^{177}Hf$	± 2SE †	ε_{Hf} ††	Sm	Nd	Lu	Hf	Sm/Nd	Lu/Hf	Nd/Hf	Nd/Lu	$^{143}Nd/^{144}Nd$ t=50 Ma †††	ε_{Nd} t = 50 Ma †††	$^{176}Hf/^{177}Hf$ t=50 Ma †††	ε_{Hf} t = 50 Ma †††
ODP Site 1201 Basement Basalts*																		
1201D46R-3 43-45	0.513054	7	8.3	0.283252	4	16.5	2.03	6.00	0.44		0.34			13.64	0.512987	8.2		
1201D46R-5 6-8	0.513077	7	8.7	0.283256	3	16.6	2.21	6.31	0.40	2.26	0.35	0.18	2.79	15.78	0.513008	8.6	0.283232	16.9
1201D48R-2 92-94	0.513134		9.8	0.283321	4	19.0	2.12	5.53	0.39		0.38			14.18	0.513058	9.6		
1201D48R-4 66-68	0.513143		10.0	0.283315	5	18.7	2.05	5.31	0.38	1.39	0.39	0.27	3.82	13.97	0.513067	9.8	0.283279	18.6
1201D49R-1 11-13	0.513148		10.1	0.283325	5	19.1	2.12	6.03	0.39	1.45	0.35	0.27	4.16	15.46	0.513079	10.0	0.283289	18.9
1201D49R-1 47-49	0.513139		9.9	0.283329	5	19.2	1.98	5.04			0.39				0.513061	9.7		
1201D49R-3 37-39	0.513135		9.9	0.283316	4	18.8	1.12	2.50	0.26	0.62	0.45	0.42	4.03	9.62	0.513046	9.4	0.283260	17.9
1201D51R-1 2 4	0.513136		9.9	0.283315	4	18.7	2.04	5.22	0.39	1.43	0.39	0.27	3.65	13.38	0.513059	9.6	0.283279	18.6
1201D52R-2-A 56-58	0.513142		10.0	0.283328	4	19.2	1.82	4.57	0.36	1.33	0.40	0.27	3.44	12.69	0.513063	9.7	0.283292	19.0
1201D53R-1 119-121	0.513139		9.9	0.283324	4	19.1	2.06	5.25	0.40	1.49	0.39	0.27	3.52	13.13	0.513061	9.7	0.283288	18.9
1201D55R-1 47-49	0.513141		10.0	0.283330	4	19.3	1.88	4.67	0.37		0.40			12.62	0.513061	9.7		
DSDP Site 447 Basement Basalts**																		
447A 14-1	0.513128	5	9.7	0.283249	4	16.4												
447A 14-2 2-4	0.513140	5	9.9	0.283248	4	16.4												
447A 16-2 22-24	0.513174	7	10.6	0.283290	4	17.9												
447A 17-2 1-4	0.513137	5	9.9	0.283297	4	18.1												
447A 17-2 53-55	0.513128	6	9.7	0.283293	5	18.0												
447A 17-3 105-107	0.513154	6	10.2	0.283293	4	18.0												
447A 21-1 128-130	0.513150		10.1	0.283306	3	18.4												
447A 22-1 60-62	0.513152	6	10.2	0.283314	3	18.7												
447A 22-3 18-20	0.513185		10.8	0.283290		17.9												
447A 23-1 16-19	0.513178	6	10.7	0.283296	4	18.1												
447A 24-2	0.513175	6	10.6	0.283264	3	16.9												
447A 25-1 15-17	0.513162	6	10.4	0.283265	4	17.0												
447A 25-1 9-11	0.513155		10.2	0.283275		17.3												
447A 30-2 80-82	0.513096		9.1	0.283268	4	17.1												
Trench Wall Forearc Basalts***																		
150-01	0.513080	2	8.8	0.283259	2	16.8	3.69	8.96	0.61	2.54	0.41	0.24	3.53	14.69	0.512999	8.4	0.283227	16.7
150-02	0.513081	2	8.8	0.283255	3	16.6	3.58	8.40	0.61	2.34	0.43	0.26	3.59	13.77	0.512997	8.4	0.283221	16.5
150-03	0.513086	2	8.9	0.283261	3	16.8	3.61	8.40	0.65	2.27	0.43	0.29	3.70	12.92	0.513001	8.5	0.283223	16.6
BT-1	0.513094	2	9.0	0.283284	4	17.6	1.41	3.05	0.27	0.81	0.46	0.33	3.77	11.30	0.513003	8.5	0.283240	17.2
BT-2	0.513086	2	8.9	0.283250	3	16.5	2.66	6.16	0.48	1.68	0.43	0.29	3.67	12.83	0.513001	8.5	0.283212	16.2
169-01a	0.513084	2	8.9	0.283279	1	17.5	1.84	4.31	0.35	1.16	0.43	0.30	3.72	12.31	0.513000	8.5	0.283239	17.2
169-01b	0.513091	2	9.0	0.283279	2	17.5	1.83	4.20	0.35	1.07	0.44	0.33	3.93	12.00	0.513005	8.6	0.283236	17.0

* Site 1201 samples are from Savov et al. (2006) with Hf isotopes from this study. Nd isotopes from Savov et al. (2006) except samples 46R-3 and 46R-5 from this study. Trace elements are from Savov et al. (2006).

**Site 447 data are from this study except Nd isotopes for samples 21-1 and 30-2 from Hickey-Vargas (1991).

**Site 447 Hf and Nd isotopes from sample 22-3 are from Pearce et al. (1999). Hf and Nd isotopes from 25-1 are from Hickey-Vargas (2006) with correction based on JMC $^{176}Hf/^{177}Hf$=0.282160

***Trench wall, forearc basalt samples are from DeBari et al. (1999). Hf and Nd isotopes are from this study. Trace elements from DeBari et al. (1999).

† Uncertainties (±) reflect within-run variation calculated as 2σ standard errors and expressed as variation in the 6th decimal place.

†† Epislon values calculated with chondritic ratios of $^{176}Hf/^{177}Hf$ = 0.282758 and $^{143}Nd/^{144}Nd$ = 0.512630 (Bouvier et al., 2008)

††† Age corrections to 50 Ma assume $^{176}Lu/^{177}Hf$ = 0.1420 and $^{147}Sm/^{144}Nd$ = 0.6042 in samples and using chondritic values for these ratios from Bouvier et al. (2008)

Chapter 5

Analytical Methods

Whole rock powders of basement basalts from Unit 1 and andesite sills from Unit IV were created at the Geological Survey of Japan, in an agate grinding container. Major element compositions for each of these were determined by XRF at the Japan Survey. Splits of the sample powders were made available for Hf and Nd isotope analysis at the University of South Carolina and ICPMS trace element analysis at Florida International University.

For Hf and Nd isotope measurements, approximately 300 mg of rock powder was weighed into Teflon capsules and leached for 30 minutes in concentrated HCl at 90-100° C. Samples were then rinsed in 18 MΩ H_2O to remove the leachate. The remaining sample was digested for 24 hours in a 3:1 HF:HNO_3 mixture. The digested samples were then heated gently on a hot plate to incipient dryness. Approximately 5 ml of concentrated HCl was then added to each sample. The capsules were sealed and heated to ~90°C for 1 hour, then uncapped and again heated to incipient dryness. This step was repeated 3 times to remove as much fluoride precipitate as possible. After the final digestion, samples were again heated to incipient dryness, cooled, and rinsed into centrifuge tubes with 5 mL of ~11 M HCl. They were centrifuged for 10 minutes at 10,000 rpm to separate the remaining solids from the liquids.

Separate aliquots were pipetted for Nd and Hf column chemistry. Neodymium was separated by cation exchange using TRU-spec resin in Teflon micro-columns,

followed by LN-spec resin micro-columns following the procedure of Hart and Brooks, (1997), and Pin and Zalduegui, (1997). Hafnium was separated using the Munker et al., (2001) method.

Isotope ratios were measured using a ThermoFinnigan Neptune ICP-MS in the Center for Elemental Mass Spectrometry at the University of South Carolina. The dissolved samples were diluted to achieve a signal of 2-5 V on ^{143}Nd and ^{176}Hf, and 30-45 analyses were run on each sample, depending on sample volume. Samples were bracketed every 4-6 solution between repeat measurements of the LaJolla standard for Nd, and the JMC457 standard for Hf. Results were normalized to a $^{143}Nd/^{144}Nd$ value of 0.511858 for LaJolla, and a $^{176}Hf/^{177}Hf$ value of 0.282160 for JMC457. Result are reported in Table 4.1. Analysis of USGS standards AGV-1, BCR-2 and BHVO-2 run as unknowns (Table 4.1) agree with values from Weis et al. (2006; 2007) to within <0.3 epsilon units. Epsilon values (ε_{Nd}, ε_{Hf}) were calculated with a CHUR value of 0.51263 for $^{143}Nd/^{144}Nd$ and 0.282785 for $^{176}Hf/^{177}Hf$ (Bouvier et al., 2008). Procedural blanks, prepared with each round of samples had an average voltage of 0.0013 V for ^{143}Nd and 0.0049 V for ^{176}Hf, while digested powders had a minimum of 0.3 V indicating an insignificant amount of contamination from processing.

Chapter 6

Results

Whole-rock major elements for the basement samples of Unit 1 and sills intruding sedimentary rocks of Unit IV are summarized in Fig. 6.1. The basement section is dominated by basalts with 47-52% SiO_2, 8-12% Fe_2O_3, 7-9% MgO, 10-14% CaO and 1.5-3.0% Na_2O (Fig. 6.1). At the top of the section, above a depth of approximately 1480 mbsf (meters below seafloor), there is a shift toward higher SiO_2 which includes 5 samples that are andesitic, with 53-57% SiO_2. These samples also have clearly lower Fe_2O_3 and CaO, and higher MgO and Na_2O than rocks deeper in the core (Fig. 6.1). For TiO_2, the basement section shows a variable and patchy distribution of compositions from 0.60 to 1.25%. In contrast, TiO_2 - P_2O_5 ratios are relatively uniform from 12 to 18, except at the top of the section where the higher SiO_2 samples shift to lower relative TiO_2, with ratios to P_2O_5 mostly below 12 (Fig. 6.1). Average loss-on-ignition (LOI) increases systematically from approximately 2% at the bottom of the basement section to more than 7% at the top. Abundances of K_2O are highly variable and appear uncorrelated with TiO_2 (Fig. 6.1). Many samples have K_2O below 0.5% and a similar number with more than 0.4% up to a maximum of approximately 1.2% (Fig. 6.1). Andesitic sills of Unit IV contain 54-55% SiO_2, with Fe_2O_3, MgO, TiO_2 and K_2O, similar to andesitic rocks from the top of the basement section (Fig. 6.1). In contrast, the andesitic sills have distinctly lower CaO and higher Na_2O, P_2O_5 and lower TiO_2-P_2O_5 ratios than any of the basement samples (Fig. 6.1).

Basement samples from Site 1438 have relatively radiogenic Hf and Nd, which are well correlated from ε_{Hf} of +14.5 to +19.5 and ε_{Nd} of +7.5 to +9.8 (Fig. 6.2). The andesite sills that intrude Unit IV sedimentary rocks fall at the less radiogenic end of this range with ε_{Hf} of +13.8 and ε_{Nd} from +6.0 to + 7.5 (Fig. 6.2). All Site 1438 compositions fall above the field of Pacific MORB in Hf-Nd isotope space and so have relatively radiogenic Hf, similar to Indian-type MORB (Fig. 6.2). Site 1201 basement basalts and northern IBM FABs of DeBari et al. (1999) are indistinguishable from Site 1438 basement with respect to Hf and Nd isotopes (Fig. 6.2). Site 447 basement basalts scatter to somewhat more radiogenic Nd, but the combined data for drill site basement samples immediately west of the KPR (Sites 1438, 1201 and 447) form a close cluster within ± 2 epsilon units of ε_{Hf} = 18 and ε_{Nd} = 9.5 (Fig. 6.2). Depleted basalts collected from IBM forearc locations and interpreted by Reagan et al. (2010) and Ishizuka et al. (2011a) be the initial products of IBM volcanism are slightly more variable with respect to Nd isotopes, but do not occupy isotopic space significantly different that defined by basement samples west of the KPR at sites 1438, 1201 and 447 (Fig. 6.2).

Incompatible trace element abundances are uniformly low in Site 1438 basement basalts, which have Hf < 1.5 ppm, Lu<0.45 ppm, Sm<2.5 ppm and Nd<6.0 ppm (Fig. 6.3). The data for Hf, Nd, Sm and Lu cluster strongly and are well correlated with TiO_2 at the depleted (low-abundance) end of the Pacific and Indian MORB fields (Fig. 6.3). Incompatible element ratios also clearly express the depleted character of Site 1438, 1201 and 447 basement samples, especially for Sm/Nd, Lu/Hf and Nd/Lu (Fig. 6.4). Incompatible trace elements and TiO_2 in some FAB samples scatter to higher TiO_2 and express less strongly depleted compositions, but the main quantity of FAB data are

strongly depleted and so appear similar to Site 1438 and other drill site basement samples west of the KPR, which are uniformly more depleted than normal MORB (Figs. 6.3-6.4).

Changes in Hf-Nd isotopes and incompatible element ratios in basement samples through time at Sites 1438, 1201 and 447 are shown in Fig. 6.5. At Site 1438, the most depleted compositions are at the bottom of the core (ε_{Nd} >9.0, ε_{Hf} >19.0). These shift to somewhat lower and more variable compositions through time. Changes in Nd/Hf, Lu/Hf, Nd/Lu and Sm/Nd also generally become less and depleted and more variable from the bottom of the Site 1438 basement section to the top (Fig. 6.5). Changes through time at Site 1201 are similar, especially with respect to Hf and Nd isotopes, which are relatively uniform and radiogenic throughout most of the basement section (ε_{Nd} = 9.0=10, ε_{Hf} >18.0-20.0) but shift to less depleted compositions at the top (Fig. 6.5). Geochemical patterns through time at Site 447 are less well constrained due to the absence of trace element data and poor sampling at the bottom of the core, which extends to a depth of 297 m below the sea floor (Fig. 6.5).

Finally, at Site 1438 we find a clear inverse correlation between incompatible element abundances and Hf – Nd isotopic composition for most basement rock data (Fig. 6.6). The pattern is particularly clear if three outlier samples with ε_{Hf}<15 and ε_{Nd}<8 are excluded. The pattern is not evident in Site 1201 basement samples, FAB or MORB datasets (not plotted).

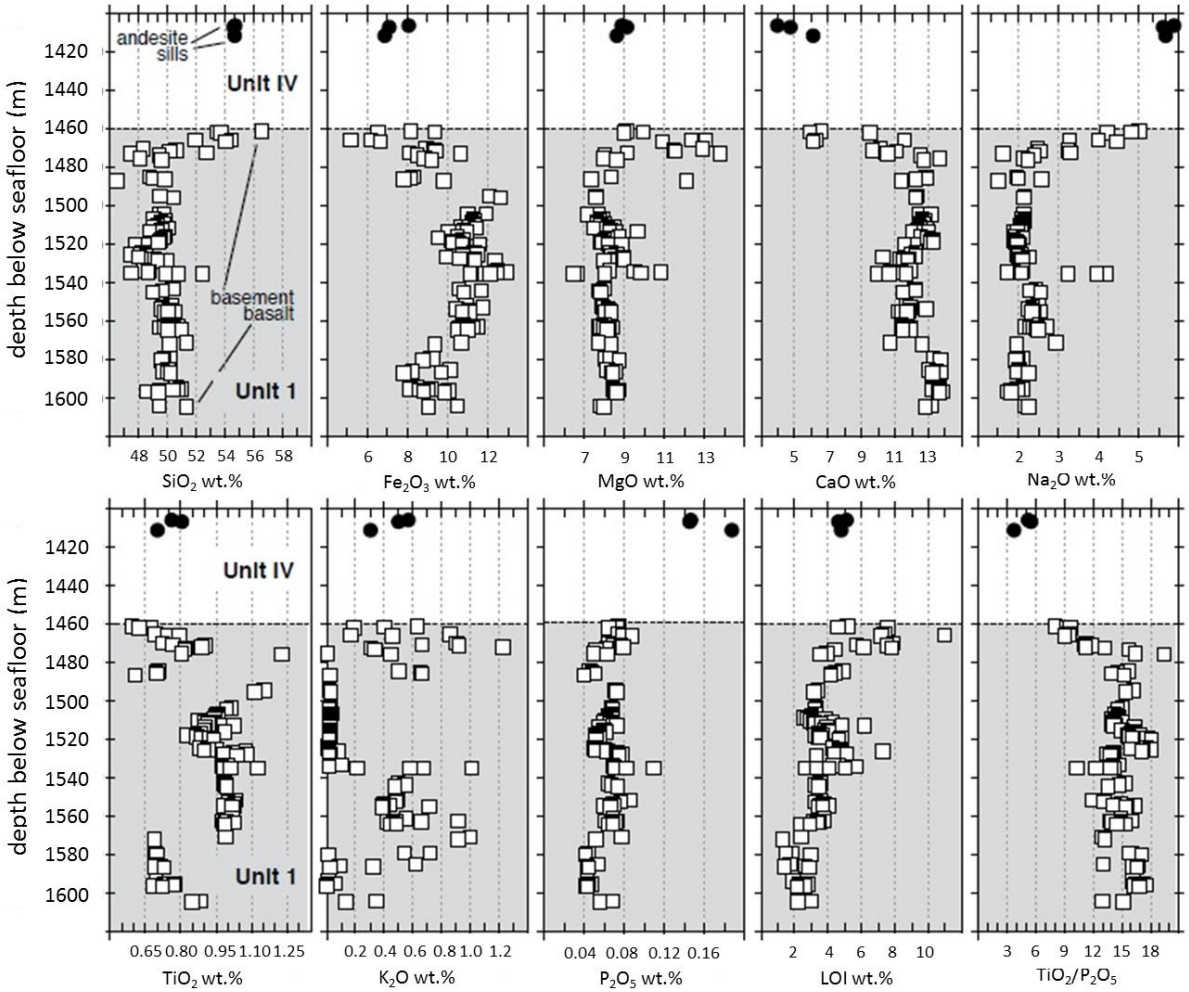

Figure 6.1 Whole rock major element composition by XRF from the Geological Survey of Japan for basement volcanic rocks and andesite sills recovered at IODP Site 1438. Data is unpublished and provided for this study courtesy of Osamu Ishizuka.

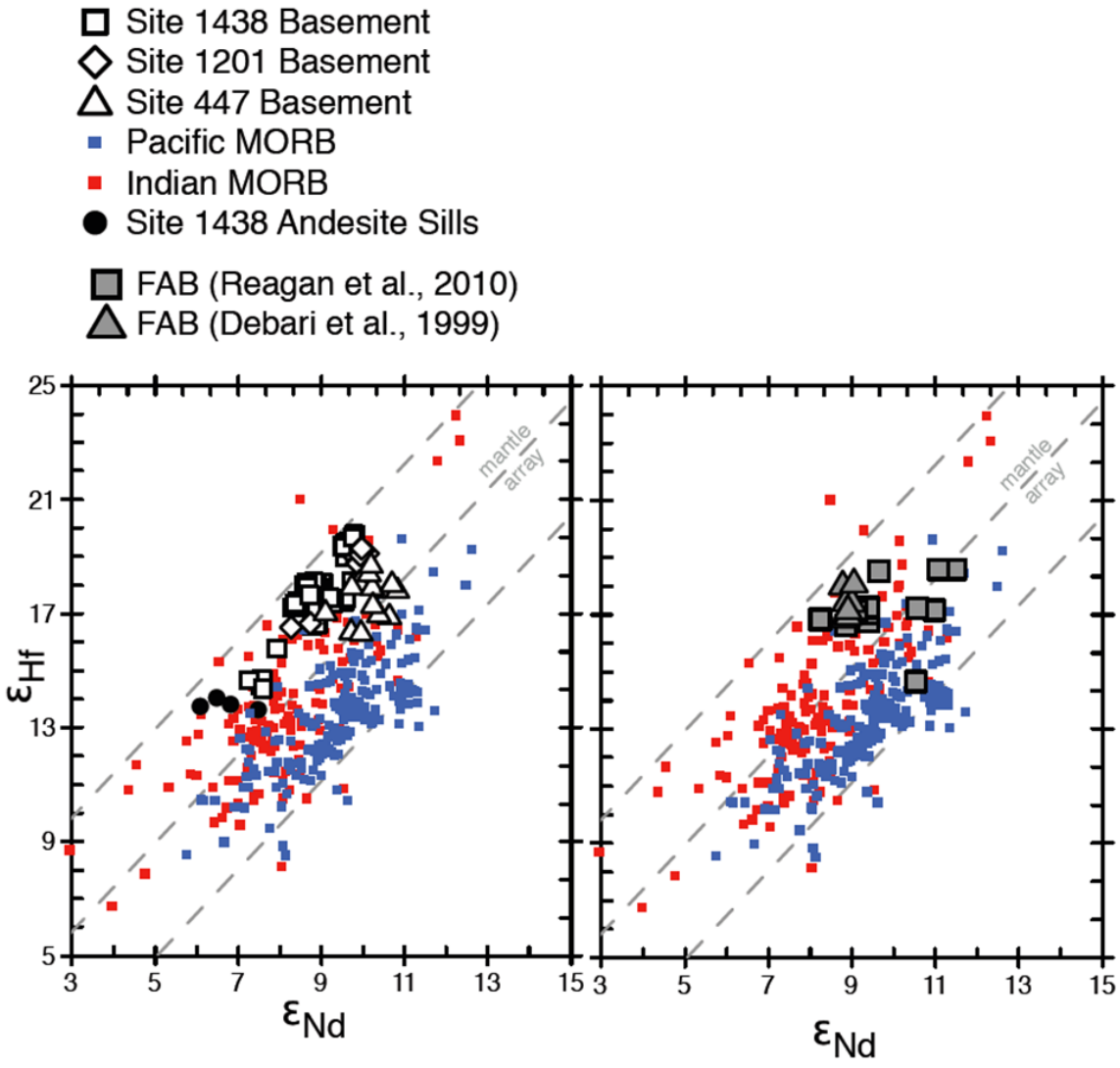

Figure 6.2. Plot of ε_{Hf} and ε_{Nd} for rocks from analyzed drill sites (data in Tables 1 and 2, including results from Savov et al., 2006, DeBari et al., 1999, Hickey-Vargas, 1991, and Hickey-Vargas et al., 2006) as well as FABs from Reagan et al. (2010) compared to Indian and Pacific MORB data from Gale et al. (2013). Samples from the backarc and forearc all plot in the same relatively small, highly depleted area of the Indian MORB field. Gray dashed lines mark the Hf-Nd isotope mantle array (center line ± 4 ε_{Hf} units) of Vervoort and Blichert-Toft (1999).

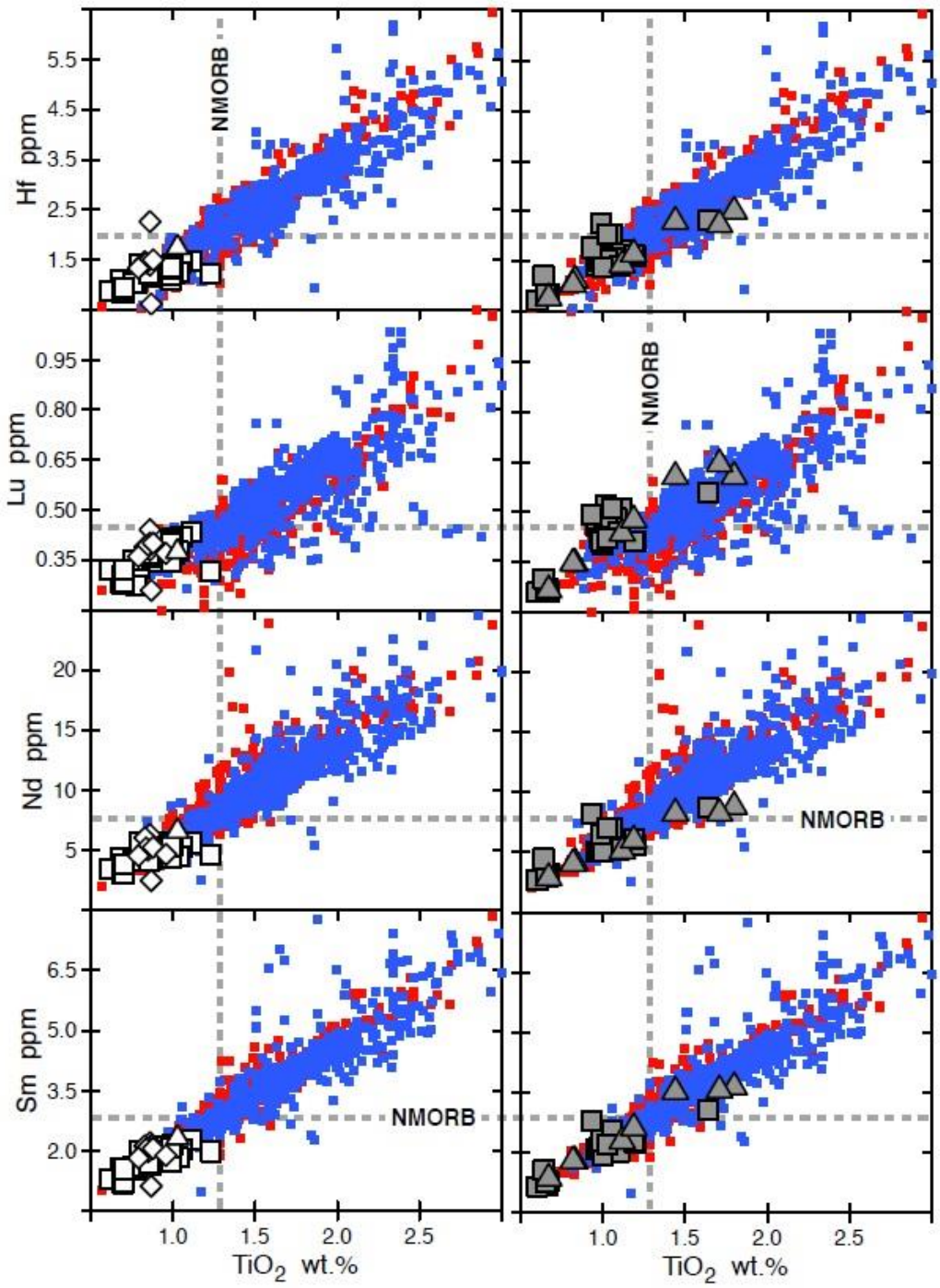

Figure 6.3. Incompatible trace element abundances compared to TiO_2 wt. % cluster strongly in a relatively uncommon highly depleted area of MORB-like basalts. They do, however, fall into the general trend of igneous processes, indicating that alteration did not cause the trace element abundances observed. Composition of normal MORB (NMORB) is from Sun and McDonough (1989). Symbols and data sources are the same as Fig. 6.2.

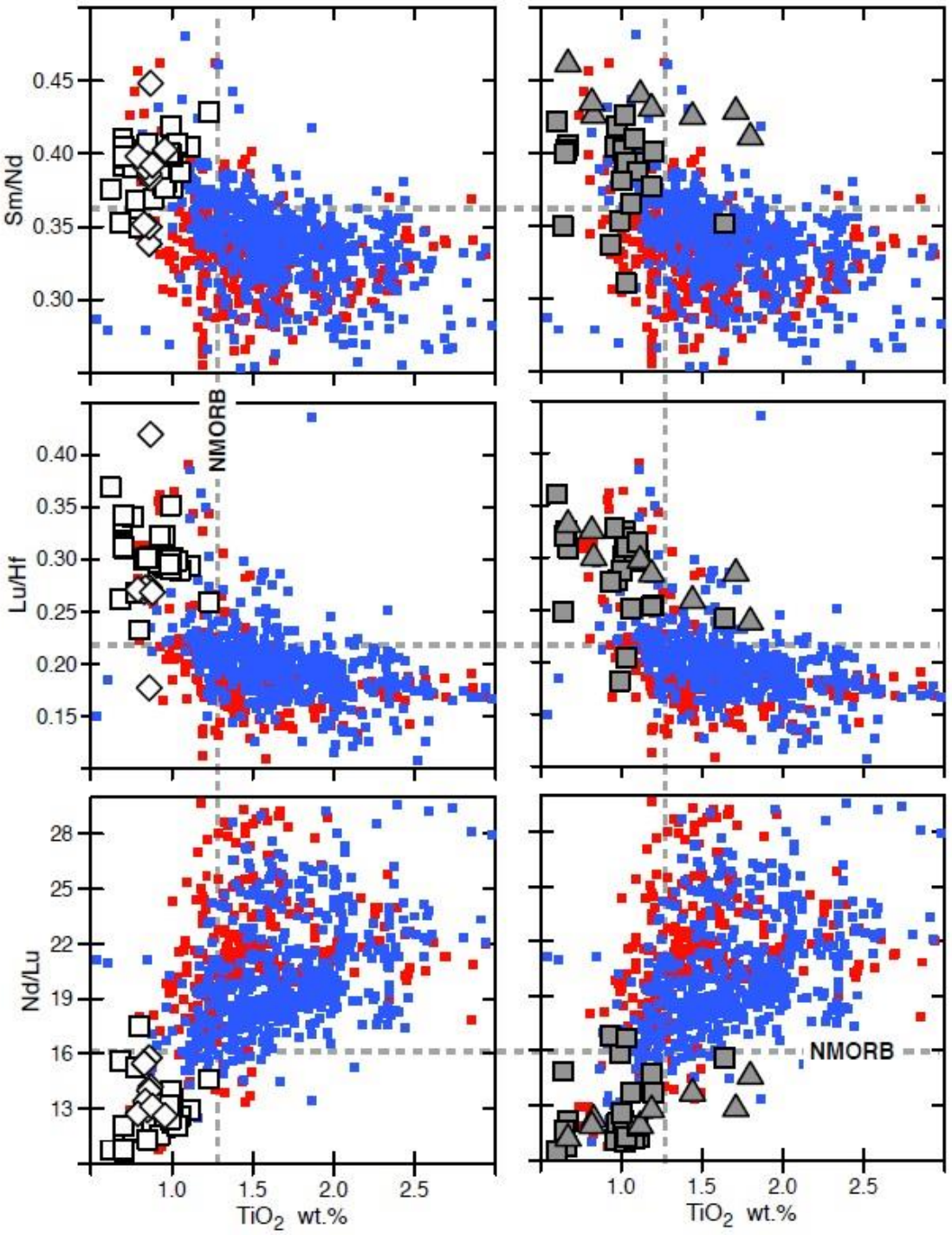

Figure 6.4. Ratios of incompatible elements support the conclusion (Fig. 6.3) that the rocks analyzed are highly depleted relative to both Pacific and Indian MORB, and are similar to one other. Composition of normal MORB (NMORB) is from Sun and McDonough (1989). Symbols and data sources are the same as Fig. 6.2.

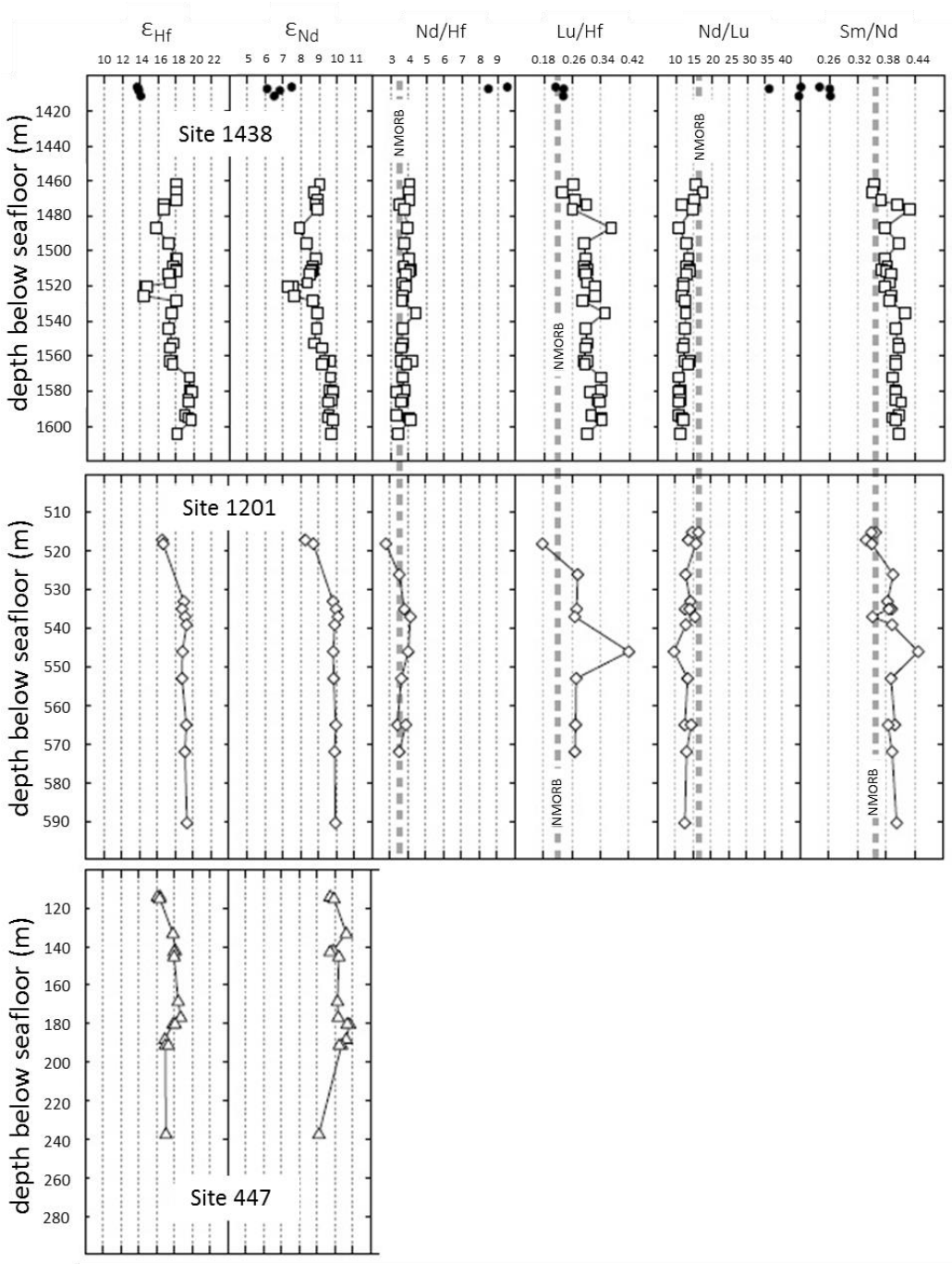

Figure 6.5. ε_{Hf}, ε_{Nd}, trace element abundances and ratios for samples from the basement of Sites 1201 and 447 show similarly depleted isotope and trace element abundance patterns to those of Site 1438 (symbols the same as in Fig. 6.1). Sites 1438 and 1201 especially, show a similar depletion in isotopes moving toward more enriched values at the top of the core. Site 447 is less clear due to a lack of samples toward the base of the core, which extends to 297 mbsf.

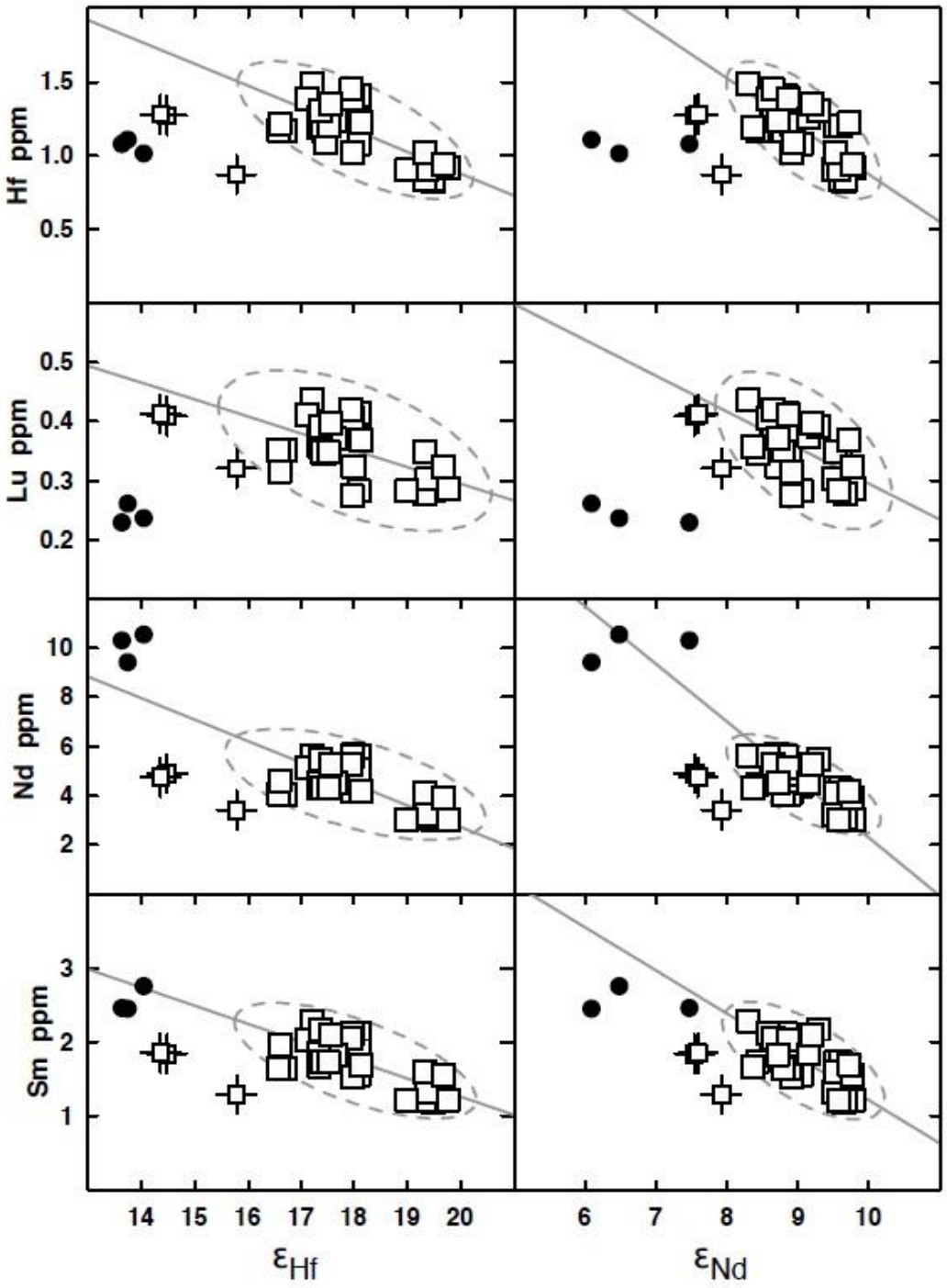

Figure 6.6. Trace element abundances versus εHf and εNd in Unit 1 basement basalts and andesite sills from Site 1438. Major axis regression lines (solid gray) through basement samples exclude three outlier with εHf<15 and εNd<8 (shown as crossed boxes). Dashed lines are major axis ellipses at 95th percentile. Data are from Table 1.

Chapter 7

Discussion

7.1 Geochemical Effects of Seawater Alteration

Changes in major element compositions at the top of the basement section toward higher SiO_2, Na_2O and MgO and lower CaO, Fe_2O_3 and TiO_2 (Fig. 6.1) are consistent with changes that would be observed if the waning stages of basement volcanism were shifted toward boninite, as observed in the IBM forearc (DeBari et al., 1999; Reagan et al., 2010; Ishizuka et al., 2011). If such a shift in basement volcanism occurred, it would be reflected in other geochemical shifts as well, especially toward lower Lu/Hf and Nd/Hf and less radiogenic Hf and Nd (ε_{Hf} <15, ε_{Nd} <8) as seen in boninites and transitional boninites highlighted by Reagan et al. (2010), Pearce et al. (1999) and others. Because these changes are not observed at Site 1438, and because the top of the basement section has a trace element character similar to normal MORB and only modestly different from the bottom (Fig. 6.5), it suggests that changes in major element compositions at the top of the section may reflect processes other than a shift in volcanic output.

One possibility is that the top of the basement section has been preferentially affected by seawater incursion and related alteration processes compared to deeper parts of the section. The progressive increase upward in LOI (loss on ignition) through the basement section is clear evidence that this process has occurred (Fig. 6.1). Samples from the top of the basement section with elevated SiO_2 and MgO have large LOIs

(4-8% - Fig. 6.1), which are inconsistent with the highly depleted trace element character of the rocks (Figs. 6.3-6.4). Such high LOIs are most easily interpreted as volatiles that were added by seawater alteration. Strong inverse correlations in plots of Nd and Hf abundances against Hf and Nd isotopes (Fig. 6.6) indicate that the primary geochemical character of the basement rocks is preserved with respect to relatively high-charge, immobile elements. The same conclusion is reached from plots of Hf and Nd abundance against TiO_2, which show strong positive correlations (Fig. 7.1). However, the chaotic appearance of K_2O when plotted against TiO_2 clearly indicates that abundances of some low-charge, and relatively fluid-mobile large ion lithophile elements do not reflect the primary igneous compositions of the rocks (Fig. 7.1). Arculus et al (2015) report strong alteration in some basement basalts, as reflected in macroscopic calcite, chlorite, sulfide and oxide minerals, which occur in patches or as veins or vesicle fillings. Such macroscopic changes could be accompanied by significant changes in bulk chemistry.

Thus, observed changes in major element compositions at the top of the basement toward higher SiO_2 and MgO and lower TiO_2 (Fig. 6.1) are tentatively interpreted to reflect alteration processes. This conclusion is pending additional petrographic observations and mineral composition data that are needed to definitively rule out the idea that major element compositions of at the top of the basement section reflect a shift toward boninite or transitional boninite compositions, as seen in some IBM forearc locations (Reagan et al., 2010).

7.2 Distinctively Depleted Source for FAB and Sites 1438 + 1201 Basement

Compositions of basement basalts at drill sites immediately west of the KPR (Sites 1438, 1201 and 447) compared to FAB samples from forearc locations east of the modern IBM arc indicate that all were derived from a similar mantle source that was geochemically distinctive and highly depleted. This is evident from the Hf isotope results for drill site basement and FAB samples, which are more radiogenic than Pacific MORB and fall at the high-ε_{Hf} end of the Indian MORB field (ε_{Hf} mostly >16.0, Fig. 6.2). It is also evident from incompatible element abundances and ratios, which are similar to the most depleted Indian and Pacific MORB compositions (Figs. 6.3-6.4). Quantitative comparisons show (1) that Site 1438 and 1201 basement basalts and FABs are indistinguishable from one-another with respect to Nd/Lu (12.9 ± 1.7 in Site samples versus 12.8 ± 1.8 in FABs) and Lu/Hf (0.300 ± 0.039 in site samples versus 0.288 ± 0.040 in FABs), and (2) that they are nonetheless more depleted than >90% of approximately 1000 published compositions of Pacific and Indian MORB (Fig. 7.2). The distinctive nature of the rocks is less clearly expressed for Sm/Nd, which is higher (more depleted) in drill site and FAB samples than in approximately 82% of Pacific and Indian MORB (Fig. 7.2). Available data indicate that basement basalts from Sites 1438 and 1201 (± 447) are, both distinctive and geochemically indistinguishable from one-another and from FABs of similar age that lie 1000-1600 km to the east and on the opposite side of the IBM orogenic system, which has been active for approximately 50 Ma. Thus, it is clear that the present-day distribution of basalts with FAB-like compositions includes a wide swath of crust that lies in the backarc along roughly 1200 km of arc length west of

the KPR (Fig. 1.1). This result affirms the findings of Arculus et al. (2015) who arrived at the same conclusion based on a much smaller set of shipboard geochemical data.

If Site 1438 basement basalts have an origin similar to FABs and were the first lavas to erupt at the time of subduction initiation, when the Pacific Plate began to sink beneath the Philippine Sea Plate 50 Ma ago (Reagan et al., 2010), then we would anticipate that some subduction-related geochemical effects may be expressed in Site 1438 basement basalts, as has been proposed for FABs (Reagan et al., 2010).

Subducted geochemical components are commonly interpreted to be aqueous fluids or melts derived from subducted sediment or seawater-altered oceanic crust (e.g., Hawkesworth et al., 1993; Kay, 1980; Morris et al., 1990; Plank & Langmuir, 1993; Turner et al., 1996). Observations of arc volcanic rocks in these studies and in and experimental melting and dehydration studies (Brenan et al., 1995; Kessel et al., 2005; Klimm et al., 2008; Spandler et al., 2007) indicate that geochemical components introduced to the mantle wedge by subduction will, in virtually all cases, be enriched in the light rare-earth elements. For Hf-Nd isotopes, the implications of this are illustrated by mantle-sediment mixing lines, which define nearly horizontal trends at the radiogenic end of the Hf-Nd isotope plot (Fig. 7.3 – blue lines). These "flat" mixing trends, reflect the high Nd/Hf character of the sediment relative to the mantle end-member. Mantle-sediment mixing will also create a coupling of Hf-Nd isotopes and certain trace element abundance ratios, including Hf/Nd and Nd/Lu, which are also not observed in the Site 1438, 1201 and FAB data (Fig. 7.4). Thus, mixing with sediment does not explain patterns in Site 1438 and related data.

Alternatively, aqueous fluids derived from seawater-altered oceanic crust in subduction zones, may introduce significant trace element variability into the source of arc volcanic rocks without creating a strong correlation with Nd or Hf isotopes (Fig. 7.4). This is because Hf-Nd isotopes are not affected by seawater alteration, so aqueous fluids produced by dewatering of altered oceanic crust may have trace element abundance ratios that contrast strongly with their MORB source, but Hf and Nd isotopes that remain like MORB. Based on bulk partitioning data from Kessel et al. (2005) an aqueous fluid extracted from MORB at 4 GPa and 700° C will have 0.48 ppm Nd and 0.04 ppm Hf (Hf/Nd=0.082). At 800° C and 4GPa, the fluid will have 1.23 ppm and 0.12 ppm Hf (Hf/Nd =0.098). Mixing of this fluid into the mantle wedge above the early IBM subducting plate would have introduced significant variability in Hf/Nd and Lu/Nd, but resulted in only limited isotopic affects. The patterns of Site 1438 and FAB data in isotope versus trace element ratio plots are consistent with this process (Fig. 7.4). Nonetheless, and as in the case of mantle-sediment mixing, the MORB fluid mixing process is unlikely to result in the steep correlation that we observe on the Hf-Nd isotope plot (Fig. 7.3). Assuming that the subducting plate in the early IBM arc had Pacific MORB geochemistry and that mixing was into a mantle wedge of Indian MORB (Pearce et al., 1999), mixing paths would again, be at a high angle to the mantle array and so unlikely to produce the well correlated and relatively steep trend of the Site 1438 data (red line in Fig. 7.2).

Thus, given the new results, and pending geochemical data more sensitive to fluid or sediment additions to a depleted mantle source (Pb, B, etc), and subject to the constraint that many samples of interest have been affected by seawater alteration, there

appears to be no evidence in the geochemistry of Site 1438 basement basalts of a geochemical component introduced by subduction recycling and mixing. A similar conclusion seems likely for FAB samples from DeBari et al. (1999), though limited isotopic variability among those samples makes this conclusion more tenuous. Enrichments in trace elements such as Cs and Rb indicate that a subduction component is present in Site 1201 basement basalts (Savov et al., 2005), but Hf, Nd, Lu and Sm abundances and ratios, combined with new data collected for this study indicate that the subduction component in Site 1201 samples has had minimal impact on Hf-Nd isotopes and rare-earth element + Hf geochemistry.

7.3 Implications for the Origin of FAB the Early IBM Arc

It is clear from results presented here that basalts with the geochemical characteristics of FAB (Reagan et al., 2010; Ishizuka et al., 2011a) were produced both east and west of the KPR in what must have been both forearc and backarc settings at the time of IBM subduction initiation. The absence of a subduction geochemical signature from Site 1438 basement samples and the presence of such a signature in forearc FABs of Reagan et al. (2010) may reflect the contrasting physical settings of volcanism in forearc (near-trench) and backarc locations (Arculus et al., 2015). However, the highly depleted aspect of the FAB geochemical signature appears to be characteristic of a highly depleted, regionally important, Indian-MORB mantle source that was sampled extensively by volcanism associated with the early IBM arc. Indeed, some basalts of the modern Izu-Bonin arc front show the same depleted compositions as Site 1438 basement, with ε_{Hf}>16.0, ε_{Nd}>9.0 and Lu/Nd>0.06 (Fig. 7.5). These rocks may be have up to 50-70

ppm Ba and Ba/La>50 from fluid enrichment above the modern subducting slab (Tamura et al., 2005), but their rare-earth element + Hf trace element patterns and Hf-Nd isotopes appear to reflect an origin in the same highly depleted mantle source from which Site 1438 basement basalts were derived. Thus, the highly depleted nature of FAB cannot be a geochemical signature uniquely associated with subduction initiation.

Source characteristics aside, the initiation of IBM subduction, and the early construction of the KPR, via widespread FAB volcanism, was contemporaneous with extensional tectonics and volcanism in a seafloor spreading-type setting that must have extended from the nascent arc front into the eastern West Philippine Basin. This type of setting fits the model of spontaneous subduction initiation proposed by Stern (2004), wherein a relatively older and more dense plate founders along a zone of weakness, possibly a fracture zone, and begins to sink under its own weight, eventually pulling itself through the asthenosphere to create a self-sustaining subduction boundary (Gurnis et al., 2004).

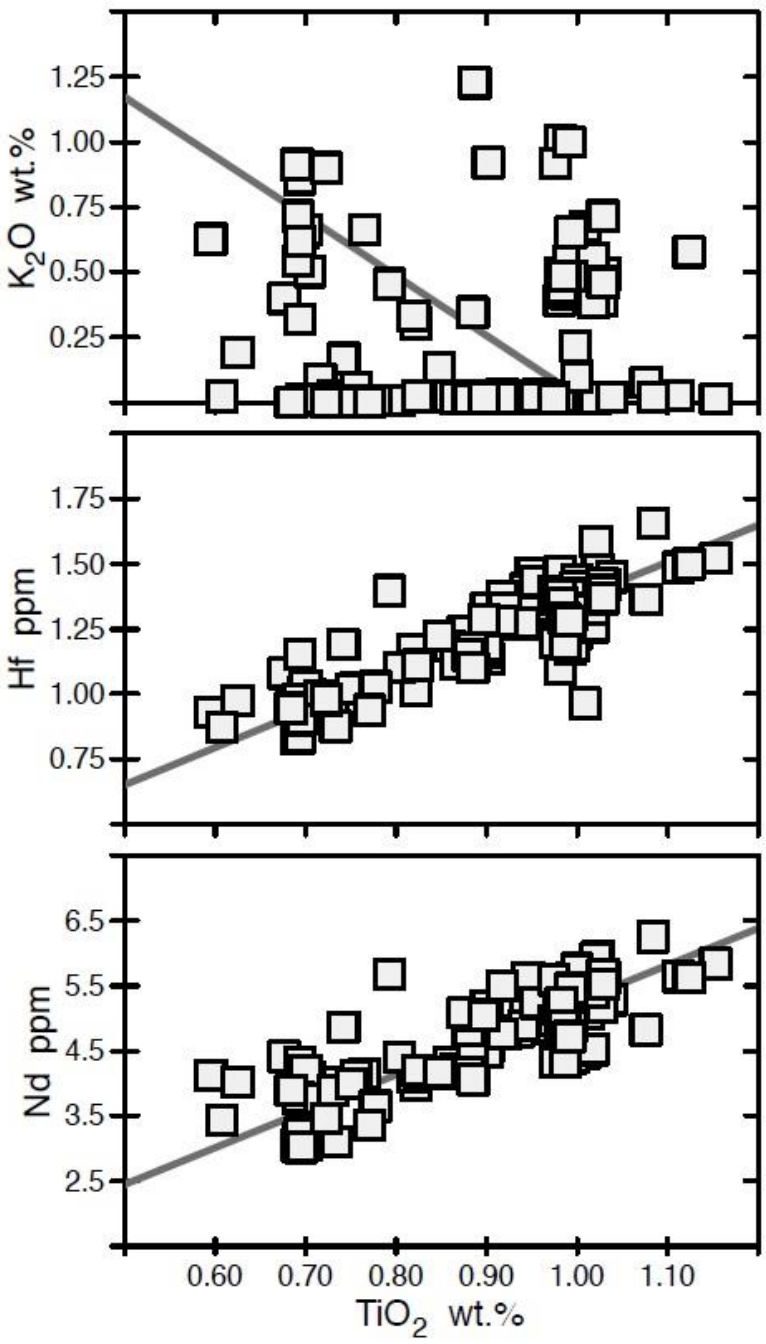

Figure 7.1 Hf, Nd, and K_2O abundances versus TiO_2. Symbols are the same as in Fig. 6.1. Solid gray lines are the reduced major axis regressions through the data.

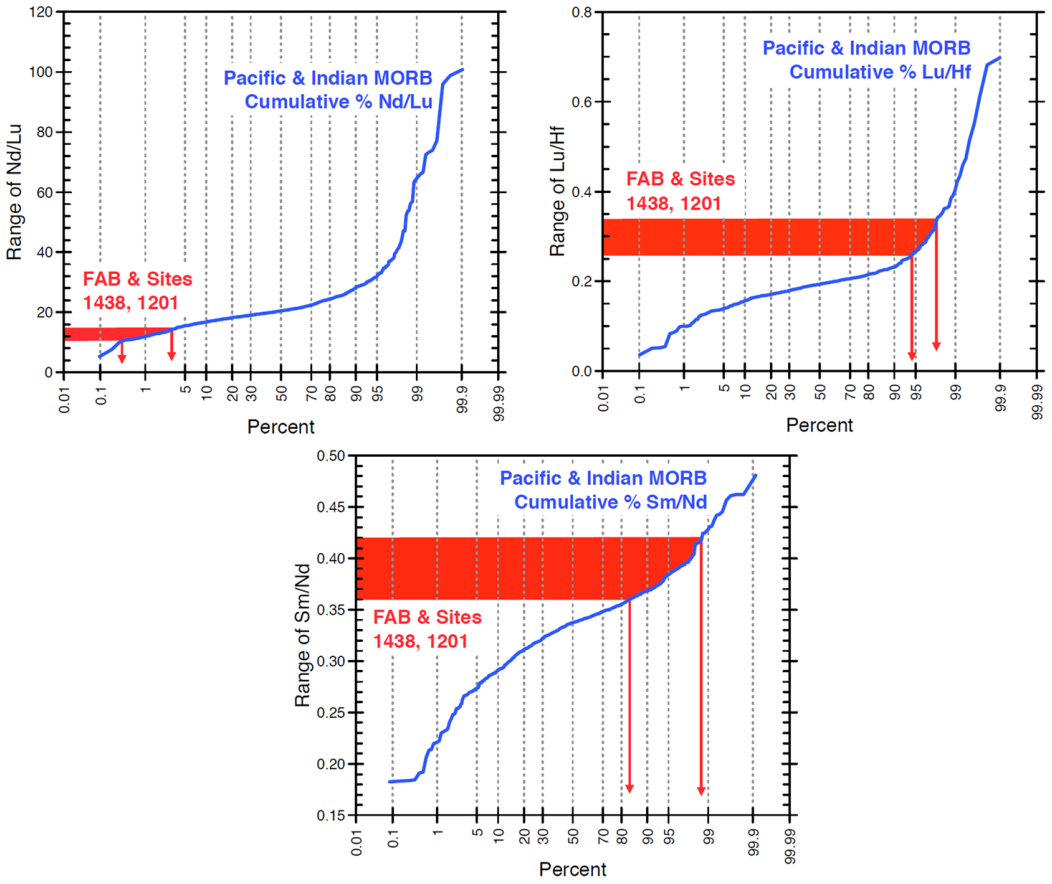

Figure 7.2 Cumulative probability curve for Nd/Lu, Lu/Hf and Sm/Nd in Pacific and Indian MORB with Site 1438 and 1201 and FAB for comparison. Blue lines are cumulative probability distributions for Pacific and Indian MORB from Gale et al. (2013). Horizontal red bars mark the combined averages for drill site basement basalts and FAB ± 1 standard deviation. Combined averages for both datasets (FAB and drill site basement) are Nd/Lu = 12.9 ± 1.7 (n=79), Lu/Hf = 0.295 ± 0.040 (n=42) and Sm/Nd = 0.392 ± 0.027 (n=79). For Indian and Pacific MORB, n = 982 for Lu/Hf, 1057 for Nd/Lu and 1175 for Sm/Nd.

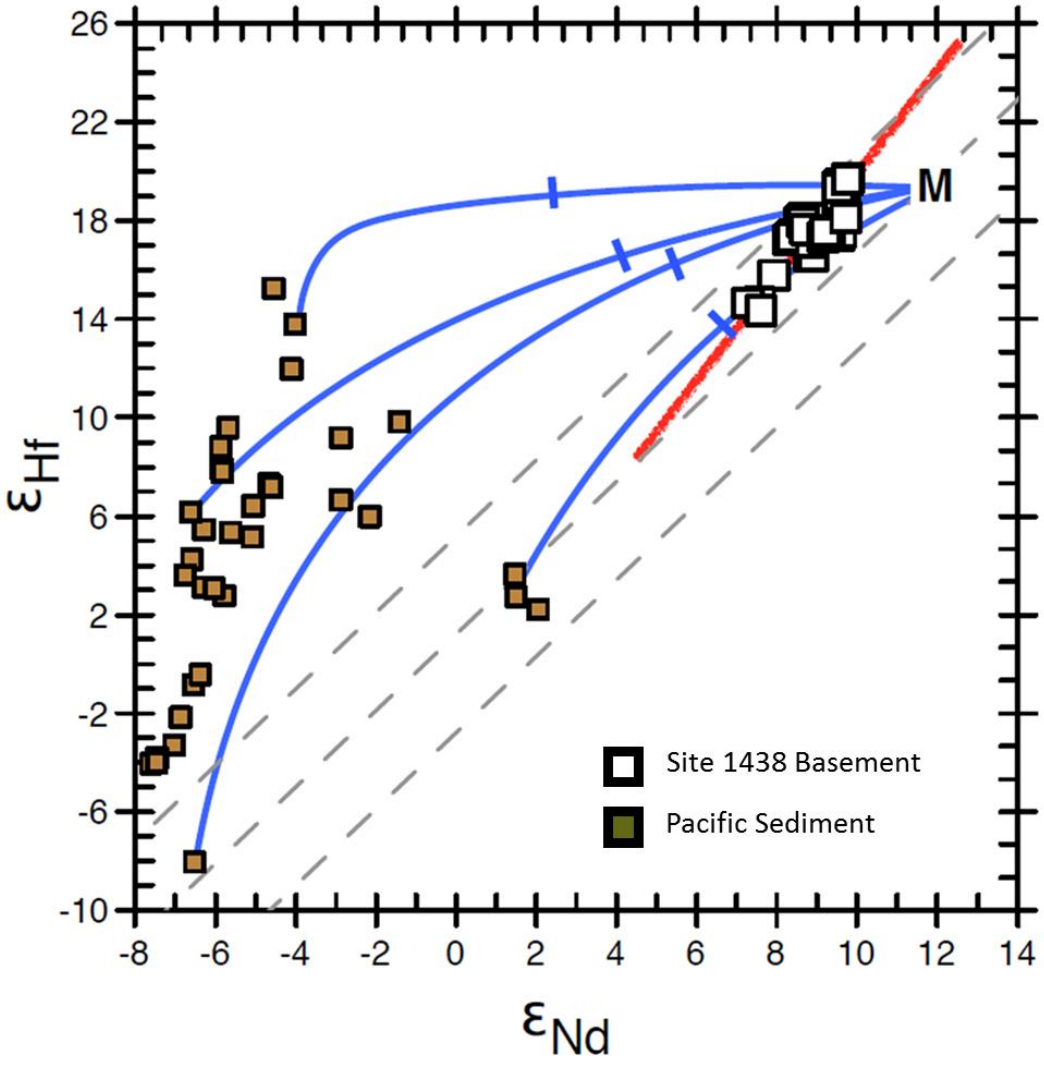

Figure 7.3 Mixing curves between Site 1438 basement and Pacific Sediments. The red line is the major axis regression through Site 1438 data. Blue lines are mixtures between mantle and various sediment end-members with tick-marks at 2.4% sediment + 97.6% mantle mixtures. Abundances for Hf and Nd in the mantle end-member (M) are from Salters & Stracke (2004). Western Pacific sediment data are from Sites 1149, 801 and 595 from Vervoort et al. (2011) and Chauvel et al. (2009).

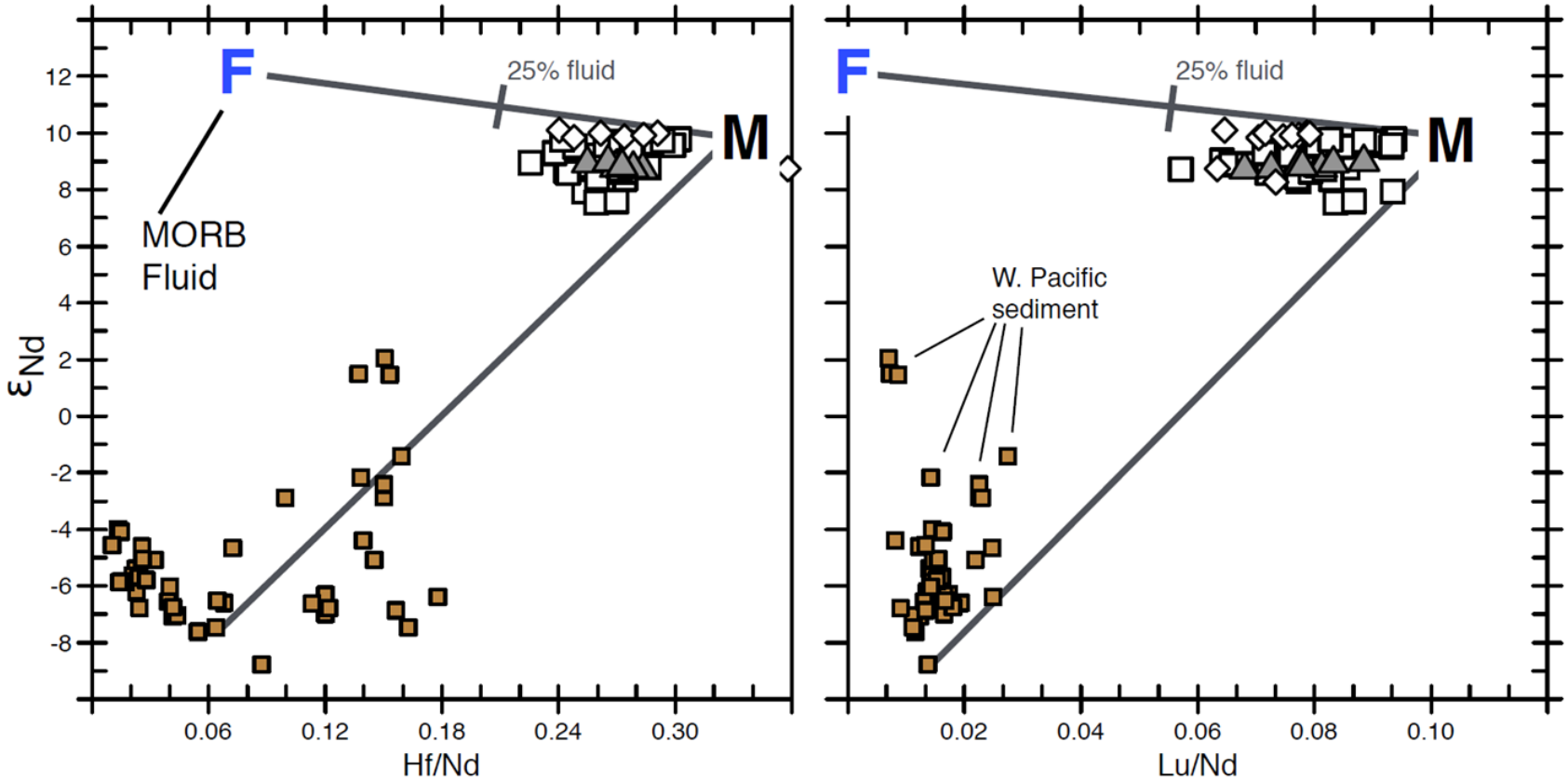

Figure 7.4 Mixing curves between Site 1438 basement and Pacific Sediments and MORB fluid. The dark gray lines are mixing lines that connect a depleted mantle composition with sediment and a MORB fluid. The tick mark on the mantle mixing line with MORB fluid is at 25% fluid. The Abundances for Hf, Nd and Lu in the mantle end-member (M) are adjusted from values of Salters & Stracke (2004) to produce Hf/Nd and Lu/Nd at the depleted end of the Site 1438 data field. The MORB fluid composition (F) has 1.23 ppm Nd, 0.12 ppm Hf and Western Pacific sediment data are from Sites 1149, 801 and 595 from Vervoort et al. (2011) and Chauvel et al. (2009). Drill site symbols are the same as Fig. 6.2.

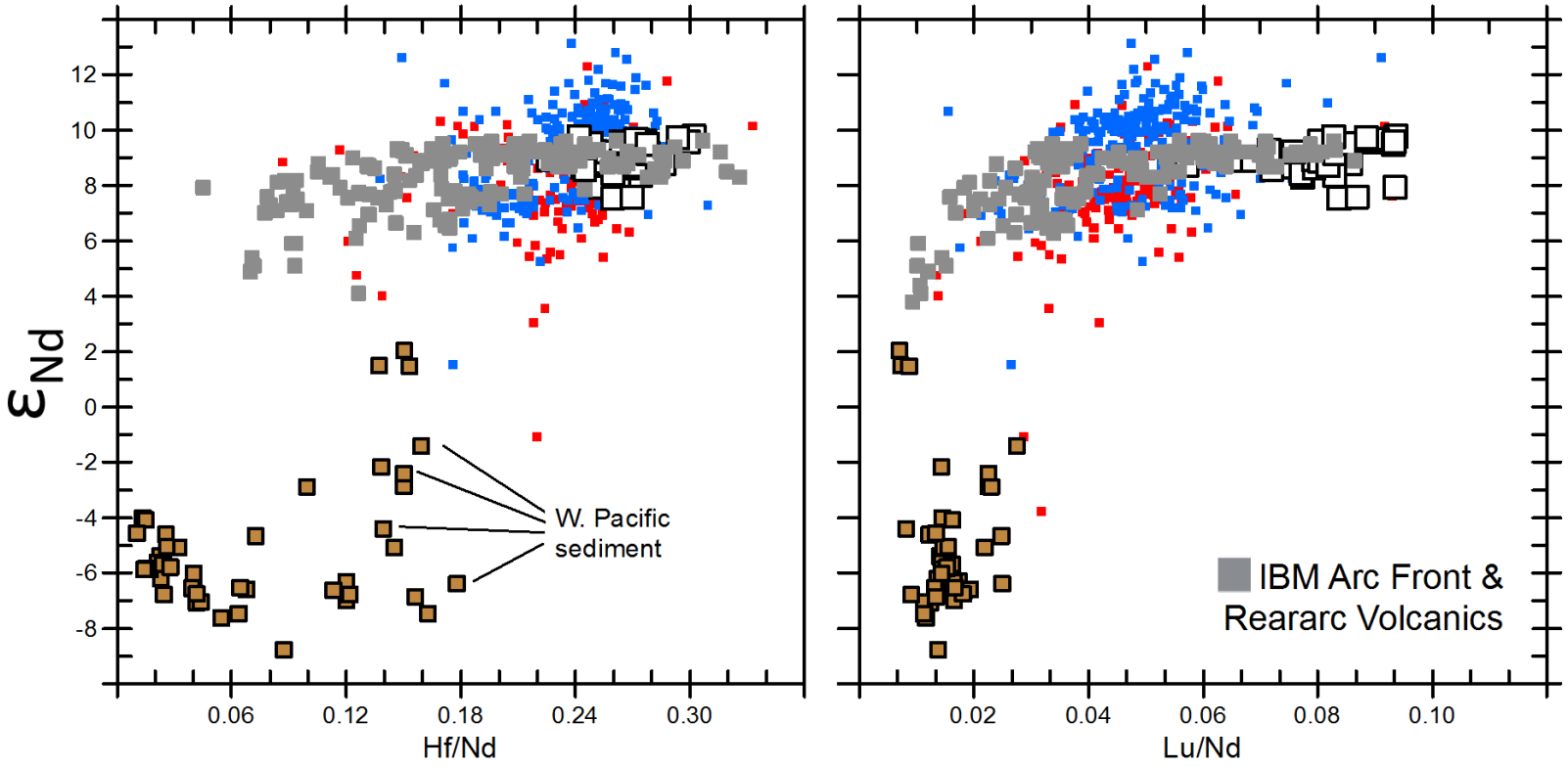

Figure 7.5 Arrays of Site 1438 basement, Pacific and Indian MORB, modern IBM arc rocks, and W. Pacific Sediments. Symbols the same as in Figs. 6.2 and 7.4. Samples from Site 1438 do not fall outside of the observed realm of MORB, or modern IBM arc rocks indicating that the IBM arc is still sampling a the highly depleted mantle source that produced Site 1438 basement with minimal input from sediments or slab derived fluids. IBM front and reararc samples are from Tamura et al., (2005, 2007), Tollstrup et al. (2010) and other published sources.

Chapter 8

Conclusion

Samples from the basement of Sites 1438 and 1201, as well as FAB samples from DeBari et al. (1999) preserve the signature of a geochemically distinctive and highly depleted mantle source. Geochemical results suggest that there was not a significant input of subducted materials (sediment, fluids) into mantle source of Site 1438 basement basalts, though additional studies of elements/isotopes more sensitive to subduction influence (Pb,?) may reveal subtle, subduction-related patterns not evident in the data presently available.

Available Hf - Nd isotope data, combined with trace element abundances for Hf, Nd, Lu, and Sm for samples from Sites 1438, 1201, and 447, as well as FABs collected in the forearc, all appear to have been derived from a common, geochemically distinctive, and highly depleted mantle source. This source was clearly present in forearc and backarc locations (east and west of the KPR) at the time of IBM subduction initiation. Since FAB geochemistry is present on both sides of the IBM system in rocks dating to the time of subduction initiation, depleted basalts that lie below the boninites in the modern IBM forearc (FABs) cannot be interpreted as the products of older, possibly Cretaceous-age spreading events that were the foundation upon which the IBM arc was built, and which became trapped in the modern forearc during rifting / arc-splitting events, as suggested by DeBari et al. (1999). Instead, basalts with FAB geochemical characteristics east and west

of the KPR all appear to have formed at the time of IBM subduction initiation (Arculus et al., 2015) or possibly much later, in the case of Site 447 basement.

The absence of a subduction geochemical signature from Site 1438 basement samples and the presence of such a signature in forearc FABs of Reagan et al. (2010) and Ishizuka et al. (2011a) may reflect the contrasting physical settings of volcanism in forearc (near-trench) and backarc locations (Arculus et al., 2015). However, the highly depleted aspect of the FAB geochemical signature appears to be characteristic of a regionally important, Indian-MORB mantle source that was sampled extensively by volcanism associated with the early IBM arc and which continues to be sampled by arc and back-arc volcanism of the modern IBM system. Thus, the highly depleted nature of FAB cannot be a geochemical signature uniquely associated with subduction initiation.

Initiation of IBM subduction, and the early construction of the KPR, via widespread FAB volcanism, was contemporaneous with extension due to seafloor spreading-type processes from the nascent arc into the eastern West Philippine Basin. This type of setting fits the model of spontaneous subduction initiation proposed by Stern (2004), wherein the older and more dense plate founders along a zone of weakness and begins to sink, eventually pulling itself through the asthenosphere until a self-sustaining subduction zone develops (Gurnis et al., 2004).

Additional data from the forearc (IODP Expedition 352; Fig. 1.1), along with more complete sampling of Sites 447 and 1201 for isotopes and trace element abundances will provide additional insight into whether the trends observed in the data currently available actually support the conclusions.

References

Arculus, R. J. et al. (2015), A record of spontaneous subduction initiation in the Izu–Bonin–Mariana arc, *Nature Geoscience*, *8*(9), 728–733, doi:10.1038/NGEO2515.

Arculus, R. J. et al. (2014), Izu-Bonin-Mariana arc origins: continental crust formation at an intra-oceanic arc: foundation, inception, and early evolution, International Ocean Discovery Program Preliminary Report, 351, doi:10.14379/iodp.pr.351.2014.

Bloomer, S. H., and J. W. Hawkins (1987), Petrology and geochemistry of boninite series volcanic rocks from the Mariana trench, *Contributions to Mineralogy and Petrology*, *97*(3), 361–377, doi:10.1007/bf00371999.

Bouvier, A., J. D. Vervoort, and P. J. Patchett (2008), The Lu–Hf and Sm–Nd isotopic composition of CHUR: Constraints from unequilibrated chondrites and implications for the bulk composition of terrestrial planets, *Earth and Planetary Science Letters*, *273*(1), 48–57, doi:10.1016/j.epsl.2008.06.010.

Brenan, J. M., H. F. Shaw, F. J. Ryerson, and D. L. Phinney (1995), Mineral-aqueous fluid partitioning of trace elements at 900°C and 2.0 GPa: Constraints on the trace element chemistry of mantle and deep crustal fluids, *Geochimica et Cosmochimica Acta*, *59*(16), 3331–3350, doi:10.1016/0016-7037(95)00215-l.

Cameron, W. E., M. T. McCulloch, and D. A. Walker (1983), Boninite petrogenesis: Chemical and Nd-Sr isotopic constraints, *Earth and Planetary Science Letters*, *65*(1), 75–89, doi:10.1016/0012-821x(83)90191-7.

Chauvel, C., J.-C. Marini, T. Plank, and J. N. Ludden (2009), Hf-Nd input flux in the Izu-Mariana subduction zone and recycling of subducted material in the mantle, *Geochemistry, Geophysics, Geosystems*, *10*(1), doi:10.1029/2008gc002101.

Cooper, P. A., and B. Taylor (1985), Polarity reversal in the Solomon Islands arc, *Nature*, *314*(4), 428–430, doi:10.1038/318391b0.

Cosca, M. A., R. J. Arculus, J. A. Pearce, and J. G. Mitchell (1998), 40Ar/ 39Ar and K-Ar geochronological age constraints for the inception and early evolution of the Izu-Bonin - Mariana arc system, *The Island Arc*, *7*(3), 579–595, doi:10.1111/j.1440-1738.1998.00211.x.

DeBari, S. M., B. Taylor, K. Spencer, and K. Fujioka (1999), A trapped Philippine Sea plate origin for MORB from the inner slope of the Izu–Bonin trench, *Earth and Planetary Science Letters*, *174*(1), 183–197, doi:10.1016/s0012-821x(99)00252-6.

Deschamps, A., and S. Lallemand (2002), The West Philippine Basin: An Eocene to early Oligocene back arc basin opened between two opposed subduction zones, *Journal of Geophysical Research: Solid Earth*, *107*(B12), doi:10.1029/2001jb001706.

Forsyth, D., and S. Uyeda (1975), On the Relative Importance of the Driving Forces of Plate Motion, Geophysical Journal International, 43(1), 163–200, doi:10.1111/j.1365-246x.1975.tb00631.x.

Gale, A., C. A. Dalton, C. H. Langmuir, Y. Su, and J.-G. Schilling (2013), The mean composition of ocean ridge basalts, *Geochemistry, Geophysics, Geosystems*, *14*(3), 489–518, doi:10.1029/2012gc004334.

Gurnis, M., C. Hall, and L. Lavier (2004), Evolving force balance during incipient subduction, *Geochemistry, Geophysics, Geosystems*, *5*(7), doi:10.1029/2003gc000681.

Hart, S. R., and C. Brooks (1977), The Geochemistry and Evolution of Early Precambrian Mantle, *Contributions to Mineralogy and Petrology*, *61*(2), 967–970, doi:10.1007/bf00374362.

Hawkesworth, C. J., K. Gallagher, J. M. Hergt, and F. McDermott (1993), Mantle and Slab Contributions in Arc Magmas, *Annual Review of Earth and Planetary Sciences*, *21*(1), 175–204, doi:10.1146/annurev.ea.21.050193.001135.

Hickey, R. L., and F. A. Frey (1982a), Rare-Earth Element Geochemistry of Mariana Fore-arc Volcanics: Deep Sea Drilling Project Site 458 and Hole 459B, *Initial Reports of the Deep Sea Drilling Project*, *60*(MAR), 735–742, doi:10.2973/dsdp.proc.60.140.1982.

Hickey, R. L., and F. A. Frey (1982b), Geochemical characteristics of boninite series volcanics: implications for their source, *Geochimica et Cosmochimica Acta*, *46*(11), 2099–2115, doi:10.1016/0016-7037(82)90188-0.

Hickey-Vargas, R. (1991), Isotope characteristics of submarine lavas from the Philippine Sea: implications for the origin of arc and basin magmas of the Philippine tectonic plate, *Earth and Planetary Science Letters*, *107*(2), 290–304, doi:10.1016/0012-821x(91)90077-u.

Hickey-Vargas, R., M. Bizimis, and A. Deschamps (2008), Onset of the Indian Ocean isotopic signature in the Philippine Sea Plate: Hf and Pb isotope evidence from Early Cretaceous terranes, *Earth and Planetary Science Letters*, *268*(3), 255–267, doi:10.1016/j.epsl.2008.01.003.

Hickey-Vargas, R., I. P. Savov, M. Bizimis, T. Ishii, and K. Fujioka (2006), Origin of diverse geochemical signatures in igneous rocks from the West Philippine Basin: Implications for tectonic models, *Geophysical Monograph- American Geophysical Union*, *166*, 287–303, doi:10.1029/166gm15.

Huene, von, R., and D. W. Scholl (1991), Observations at convergent margins concerning sediment subduction, subduction erosion, and the growth of continental crust, *Reviews of Geophysics*, *29*(3), 279–316, doi:10.1029/91rg00969.

Ishizuka, O., K. Tani, M. K. Reagan, K. Kanayama, S. Umino, Y. Harigane, I. Sakamoto, Y. Miyajima, M. Yuasa, and D. J. Dunkley (2011a), The timescales of subduction initiation and subsequent evolution of an oceanic island arc, *Earth and Planetary Science Letters*, *306*(3), 229–240, doi:10.1016/j.epsl.2011.04.006.

Ishizuka, O., R. N. Taylor, M. Yuasa, and Y. Ohara (2011b), Making and breaking an island arc: A new perspective from the Oligocene Kyushu-Palau arc, Philippine Sea, *Geochemistry, Geophysics, Geosystems*, *12*(5), doi:10.1029/2010gc003440.

Jenner, F. E., and H. Saint C. O'Neill (2012), Analysis of 60 elements in 616 ocean floor basaltic glasses, *Geochemistry, Geophysics, Geosystems*, *13*(2), doi:10.1029/2011gc004009.

Karig, D. E. (1975), Basin Genesis in the Philippine Sea, *Initial Reports of the Deep Sea Drilling Project*, *31*, 857–879, doi:10.2973/dsdp.proc.31.142.1975.

Kay, R. W. (1980), Volcanic Arc Magmas: Implications of a Melting-Mixing Model for Element Recycling in the Crust-Upper Mantle System, *The Journal of Geology*, *88*(5), 497–552, doi:10.1086/628541.

Kelley, K. A., T. Plank, J. Ludden, and H. Staudigel (2003), Composition of altered oceanic crust at ODP Sites 801 and 1149, *Geochemistry, Geophysics, Geosystems*, *4*(6), doi:10.1029/2002gc000435.

Kessel, R., P. Ulmer, T. Pettke, M. W. Schmidt, and A. B. Thompson (2005), The water–basalt system at 4 to 6 GPa: Phase relations and second critical endpoint in a K-free eclogite at 700 to 1400 °C, *Earth and Planetary Science Letters*, *237*(3), 873–892, doi:10.1016/j.epsl.2005.06.018.

Kobayashi, K., and M. Nakada (1978), Magnetic Anomalies And Tectonic Evolution Of The Shikoku Inter-Arc Basin, *Journal of Physics of the Earth*, *26*(Supplement), S391–S402, doi:10.4294/jpe1952.26.supplement_s391.

McKenzie, D. P. (1969), Speculations on the Consequences and Causes of Plate Motions, *Geophysical Journal International*, *18*(1), 1–32, doi:10.1111/j.1365-246x.1969.tb00259.x.

Meijer, A. (1980), Primitive arc volcanism and a boninite series: Examples from western Pacific island arcs, *The tectonic and geologic evolution of Southeast Asian seas and islands*, 269–282, doi:10.1029/gm023p0269.

Morris, J. D., W. P. Leeman, and F. Tera (1990), The subducted component in island arc lavas: constraints from Be isotopes and B–Be systematics, *Nature*, *344*(6261), 31–36, doi:10.1038/344031a0.

Münker, C., S. Weyer, E. Scherer, and K. Mezger (2001), Separation of high field strength elements (Nb, Ta, Zr, Hf) and Lu from rock samples for MC-ICPMS measurements, *Geochemistry, Geophysics, Geosystems*, *2*(12), doi:10.1029/2001gc000183.

Pearce, J.A., P.D.Kempton, G.M. Nowell, and S.R. Noble. (1999), Hf-Nd Element and Isotope Perspective on the Nature and Provenance of Mantle and Subduction Components in Western Pacific Arc-Basin Systems, *Journal of Petrology*, *40*(11), 1579–1611, doi:10.1093/petrology/40.11.1579.

Pin, C., and J. F. S. Zalduegui (1997), Sequential separation of light rare-earth elements, thorium and uranium by miniaturized extraction chromatography: Application to isotopic analyses of silicate rocks, *Analytica Chimica Acta*, *339*(1), 79–89, doi:10.1016/s0003-2670(96)00499-0.

Plank, T., and C. H. Langmuir (1993), Tracing trace elements from sediment input to volcanic output at subduction zones, *Nature*, *362*(6422), 739–743, doi:10.1038/362739a0.

Reagan, M. K. et al. (2010), Fore-arc basalts and subduction initiation in the Izu-Bonin-Mariana system, *Geochemistry, Geophysics, Geosystems*, *11*(3), doi:10.1029/2009gc002871.

Salters, V. J. M., and A. Stracke (2004), Composition of the depleted mantle, *Geochemistry, Geophysics, Geosystems*, *5*(5), doi:10.1029/2003gc000597.

Savov, I. P., R. Hickey-Vargas, M. D'Antonio, J. G. Ryan, and P. Spadea (2006), Petrology and Geochemistry of West Philippine Basin Basalts and Early Palau-Kyushu Arc Volcanic Clasts from ODP Leg 195, Site 1201D: Implications for the Early History of the Izu-Bonin-Mariana Arc, *Journal of Petrology*, *47*(2), 277–299, doi:10.1093/petrology/egi075.

Seno, T., and S. Maruyama (1984), Paleogeographic reconstruction and origin of the Philippine Sea, *Tectonophysics*, *102*(1), 53–84, doi:10.1016/0040-1951(84)90008-8.

Shervais, J. W. (1982), Ti-V plots and the petrogenesis of modern and ophiolitic lavas, *Earth and Planetary Science Letters*, *59*(1), 101–118, doi:10.1016/0012-821x(82)90120-0.

Spandler, C., J. Mavrogenes, and J. Hermann (2007), Experimental constraints on element mobility from subducted sediments using high-P synthetic fluid/melt inclusions, *Chemical Geology*, *239*(3), 228–249, doi:10.1016/j.chemgeo.2006.10.005.

Staudigel, H., G. R. Davies, S. R. Hart, K. M. Marchant, and B. M. Smith (1995), Large scale isotopic Sr, Nd and O isotopic anatomy of altered oceanic crust: DSDP/ODP sites417/418, *Earth and Planetary Science Letters*, *130*(1), 169–185, doi:10.1016/0012-821x(94)00263-x.

Stern, R. J. (2004), Subduction initiation: spontaneous and induced, *Earth and Planetary Science Letters*, *226*(3), 275–292, doi:10.1016/j.epsl.2004.08.007.

Sun, S. S., and W. F. McDonough (1989), Chemical and isotopic systematics of oceanic basalts: implications for mantle composition and processes, *Geological Society, London, Special Publications*, *42*(1), 313–345, doi:10.1144/gsl.sp.1989.042.01.19.

Sutter, J. F., and L. W. Snee (1981), K/Ar and 40Ar/39Ar Dating of Basaltic Rocks from Deep Sea Drilling Project Leg 59, *Initial Reports of the Deep Sea Drilling Project*, *59*, 729–734, doi:10.2973/dsdp.proc.59.133.1981.

Tamura, Y. (2005), Are Arc Basalts Dry, Wet, or Both? Evidence from the Sumisu Caldera Volcano, Izu-Bonin Arc, Japan, *Journal of Petrology*, *46*(9), 1769–1803, doi:10.1093/petrology/egi033.

Tamura, Y., K. Tani, Q. Chang, H. Shukuno, H. Kawabata, O. Ishizuka, and R. S. Fiske (2007), Wet and Dry Basalt Magma Evolution at Torishima Volcano, Izu Bonin Arc, Japan: the Possible Role of Phengite in the Downgoing Slab, *Journal of Petrology*, *48*(10), 1999–2031, doi:10.1093/petrology/egm048.

Taylor, B., and A. M. Goodliffe (2004), The West Philippine Basin and the initiation of subduction, revisited, *Geophysical Research Letters*, *31*(12), doi:10.1029/2004gl020136.

Thompson, P.M.E., P. D. Kempton, and A. C. Kerr (2008), Evaluation of the effects of alteration and leaching on Sm–Nd and Lu–Hf systematics in submarine mafic rocks, Lithos, 104(1-4), 164–176, doi:10.1016/j.lithos.2007.12.005.

Tollstrup, D., J. Gill, A. Kent, D. Prinkey, R. Williams, Y. Tamura, and O. Ishizuka (2010), Across-arc geochemical trends in the Izu-Bonin arc: Contributions from the subducting slab, revisited, *Geochemistry, Geophysics, Geosystems*, *11*(1), n/a, doi:10.1029/2009gc002847.

Turner, S., C. Hawkesworth, P. van Calsteren, E. Heath, R. Macdonald, and S. Black (1996), U-series isotopes and destructive plate margin magma genesis in the Lesser Antilles, *Earth and Planetary Science Letters*, *142*(1), 191–207, doi:10.1016/0012-821x(96)00078-7.

Vervoort, J. D., T. Plank, and J. Prytulak (2011), The Hf–Nd isotopic composition of marine sediments, *Geochimica et Cosmochimica Acta*, *75*(20), 5903–5926, doi:10.1016/j.gca.2011.07.046.

Vervoort, J. D., and J. Blichert-Toft (1999), Evolution of the depleted mantle: Hf isotope evidence from juvenile rocks through time, *Geochimica et Cosmochimica Acta*, *63*(3), 533–556, doi:10.1016/s0016-7037(98)00274-9.

Wang, J., T. Kusky, L. Wang, A. Polat, and H. Deng (2015), A Neoarchean subduction polarity reversal event in the North China Craton, *Lithos*, *220*, 133–146, doi:10.1016/j.lithos.2015.01.029.

Weis, D. et al. (2006), High-precision isotopic characterization of USGS reference materials by TIMS and MC-ICP-MS, *Geochemistry, Geophysics, Geosystems*, *7*(8), n/a, doi:10.1029/2006gc001283.

Weis, D., B. Kieffer, D. Hanano, I. N. Silva, J. Barling, W. Pretorius, C. Maerschalk, and N. Mattielli (2007), Hf isotope compositions of U.S. Geological Survey reference materials, *Geochemistry, Geophysics, Geosystems*, *8*(6), n/a, doi:10.1029/2006gc001473.